NACA

RESEARCH MEMORANDUM

AERODYNAMIC DESIGN OF AXIAL-FLOW COMPRESSORS

VII - BLADE-ELEMENT FLOW IN ANNULAR CASCADES

By William H. Robbins, Robert J. Jackson, and Seymour Lieblein

Lewis Flight Propulsion Laboratory
Cleveland, Ohio

CLASSIFICATION CHANGE

To Unclassified

By authority of _____

Changed by _____ Date _____

NATIONAL ADVISORY COMMITTEE
FOR AERONAUTICS
WASHINGTON

Restriction/Classification Cancelled

CONFIDENTIAL

TABLE OF CONTENTS

CONFIDENTIAL

NATIONAL ADVISORY COMMITTEE FOR AERONAUTICS

RESEARCH MEMORANDUM

AERODYNAMIC DESIGN OF AXIAL-FLOW COMPRESSORS

VII - BLADE-ELEMENT FLOW IN ANNULAR CASCADES

By William H. Robbins, Robert J. Jackson, and Seymour Lieblein

SUMMARY

A blade-element analysis is made of annular-cascade data obtained primarily from single-stage compressor test installations. The parameters that describe blade-element flow (total-pressure loss, incidence angle, and deviation angle) are discussed with reference to the many variables affecting these parameters. The blade-element data are correlated over a fairly wide range of inlet Mach number and cascade geometry. Two blade shapes are considered in detail, the 65-series profile and the double-circular-arc airfoil. Compressor data at three radial positions near the tip, mean, and hub are correlated at minimum-loss incidence angle. Curves of loss, incidence angle, and deviation angle are presented for rotor and stator blade elements. These correlation curves are presented in such a manner that they are directly related to the low-speed two-dimensional-cascade results. As far as possible, physical explanations of the flow phenomena are presented. In addition, a calculation procedure is given to illustrate how the correlation curves could be utilized in compressor design.

INTRODUCTION

Axial-flow-compressor research has generally been directed toward the solution of either compressor design or compressor analysis problems. In the design problem, the compressor-inlet and -outlet conditions are given, and the compressor geometry must be determined to satisfy these conditions. In contrast, for the analysis problem the inlet conditions and compressor are specified, and the outlet conditions are desired. (The analysis problem is sometimes referred to as the "direct compressor problem.")

There are two phases of the axial-flow-compressor design problem. In the first phase it is necessary to prescribe desirable velocity distributions at each radius of the compressor that will ultimately fulfill the design requirements. A detailed discussion of the velocity-diagram

phase of the compressor design procedure is given in reference 1. Secondly, proper blade sections are selected at each radial position and stacked in proper relation to each other to establish the design velocity diagrams at each radius. In order to satisfy the design requirements successfully, accurate blade row design data are needed. Successful analysis of a compressor (the analysis problem) also depends upon accurate blade-row data, not only at the design point but also over a wide range of flow conditions (ref. 2).

In general, compressor designers have relied primarily on three sources of blading information: (1) theoretical (potential-flow) solutions of the flow past airfoil cascades, (2) low-speed two-dimensional-cascade data, and (3) three-dimensional annular-cascade data. Potential-flow solutions have been used to a limited extent. In order to handle the complex mathematics involved in the theoretical solutions, it is necessary to make simplifying assumptions concerning the flow field. Among the most important of these is the assumption of a two-dimensional flow field with no losses. Unfortunately, in some cases these assumptions lead to invalid results unless experimental correction factors are applied to the computed results. These solutions are reviewed in reference 3.

A considerable amount of blade design data has been obtained from low Mach number experimental two-dimensional cascades. A rather complete history of the cascade work that has been done to date is presented in reference 4, which correlates cascade data at minimum-loss incidence angle for a wide range of inlet conditions and blade loadings. Low-speed two-dimensional-cascade data have been applied successfully in many compressor designs. However, with the design trends toward higher Mach numbers and higher blade loadings, these cascade results have not always been completely adequate for describing the compressor flow conditions, particularly in regions of the compressor where three-dimensional flow effects predominate.

Because of such effects, it becomes essential that blade-element data be obtained in a three-dimensional compressor environment. These three-dimensional-cascade data (obtained primarily from single-stage compressors) may then be used to supplement and correct the theoretical solutions and the two-dimensional-cascade information. Some success has been obtained in correlating annular-cascade data with the theory and the two-dimensional-cascade results (refs. 5 to 9); however, the range of variables covered in these investigations is not nearly complete.

The purpose of this report is to correlate and summarize the available compressor data on a blade-element basis for comparison with the two-dimensional-cascade data of reference 4. An attempt is made to indicate the regions of a compressor where low-speed two-dimensional-cascade data can be applied to compressors and also to indicate the regions where cascade results must be modified for successful application to compressor

design. Two blade sections are considered in detail, the NACA 65-series blade and the double-circular-arc airfoil section. Particular emphasis is placed on obtaining incidence angle, deviation angle, and loss correlations at minimum loss for blade elements near the hub, mean, and tip radii of both rotor and stator blades. Empirical correction factors that can be applied to the two-dimensional-cascade design rules are given, and application of the design rules and correction factors to compressor design is illustrated.

PRELIMINARY CONSIDERATIONS

Blade-Element Concept

In current design practice, the flow distribution at the outlet of compressor blade rows is determined from the flow characteristics of the individual blade sections or elements. The blade-element approach to compressor design is discussed in detail in references 10 and 11. To review briefly, axial-flow-compressor blades are evolved from a process of radial stacking of individual airfoil shapes called blade elements. The blade elements are assumed to be along surfaces of revolution generated by rotating a streamline about the compressor axis; this stream surface of revolution may be approximated by an equivalent cone (fig. 1). Each element along the height of the blade is designed to direct the flow of air in a certain direction as required by the design velocity diagram of the blade row. The basic parameters defining the flow about a blade element are indicated in figure 2. Stated simply, blade-element flow is described by the variations of the loss in total pressure across the blade row and of the air turning angle with the incidence angle (or angle of attack).

Factors Affecting Blade-Element Performance

The flow about a given blade element in a compressor configuration is different from that in a two-dimensional cascade because of three-dimensional effects in compressor blade rows. These three-dimensional effects influence the magnitude of the design incidence angle, the loss in total pressure, and the deviation angle.

Incidence angle. - In the low-speed two-dimensional cascade, the minimum-loss incidence angle depends on the blade geometry (camber, solidity, and blade thickness), the inlet-air angle, and inlet Mach number (ref. 4). In compressor operation, several additional factors can alter the minimum-loss incidence angle for a given element geometry - for example, differences in testing procedure. In compressor operation, incidence angle, inlet-air angle, and inlet Mach number vary simultaneously; in contrast, cascades are often operated with fixed inlet-air angle and

inlet Mach number. Some net difference in the range characteristics and, therefore, the location of the point of minimum loss between cascade oper-ation at constant inlet-air angle and compressor test operation (with varying inlet-air angle) may be obtained.

In addition to these blade-element considerations, of course, there are sources of difference arising from compressor three-dimensional ef-fects. For example, a change of minimum-loss incidence angle has been observed in the compressor rotor as radial position is varied (refs. 12 and 13), but cascade and compressor blade-element minimum-loss incidence angles have not been compared over a wide range of blade loadings and in-let Mach numbers.

Total-pressure loss. - In the two-dimensional cascade, the magnitude of the loss in total pressure across the blade element is determined from the growth of the blade-surface boundary layers (profile loss). In the actual compressor, the loss in total pressure is determined not only by the profile loss, but also by the losses induced by the three-dimensional nature of the flow. These three-dimensional losses result from secondary motions and disturbances generated by the casing wall boundary layers, from blade tip clearance, from radial gradients of total energy, and from interactions of adjacent blade rows. The compressor loss picture is fur-ther complicated by the tendency of boundary-layer fluid on the compres-sor blade surfaces and in the blade wake to be displaced radially. As a consequence of this phenomenon, the loss measured downstream of a given blade element may not necessarily reflect the actual loss generated at that element, but something more or less, depending on the radial loca-tion of the element.

It is expected, therefore, that the factors influencing the magni-tude of the blade-element loss in the compressor will include the factors affecting the profile loss (blade-surface velocity distribution, inlet Mach number, blade-chord Reynolds number, free-stream turbulence, and blade surface finish) and the factors affecting the three-dimensional losses. Investigations of compressor blade-element losses based on sur-face velocity distribution, as expressed in terms of diffusion factors, are presented in references 14 and 15. The essentially secondary effects of blade surface finish and trailing-edge thickness on compressor loss are investigated in references 16 and 17. Results of tests of blade-element performance (ref. 18) and over-all performance (refs. 19 to 21) at varying Reynolds numbers indicate that there is no significant varia-tion in loss for Reynolds numbers above approximately 2.5×10^5. (Since most of the compressor data used in this analysis are for Reynolds num-bers greater than 2.5×10^5, no Reynolds number effects are believed to exist for the data.) The variations of compressor loss with inlet Mach number have been established in references 12, 22, and 23. These results, however, are not complete indications of Mach number effects (shock losses), since the corresponding variations of blade diffusion with Mach

number are not identified. An attempt to separate the variation of diffusion and shock losses with Mach number by means of an analysis based on the diffusion factor of reference 14 is presented in references 13 and 24.

Although some aspects of the compressor three-dimensional flow phenomena are known (refs. 25 and 26), the specific factors or parameters affecting compressor three-dimensional losses have not been established for analysis purposes. At present, the three-dimensional loss can be treated only on a gross basis as a difference between the total measured loss and the predicted profile loss.

Deviation angle. - In the two-dimensional cascade the minimum-loss deviation angle varies primarily with the blade geometry and the inlet-air angle. Experience with compressor operation indicates that blade-element minimum-loss deviation angle is also sensitive to three-dimensional effects. The two principal compressor effects are secondary flows and changes in axial velocity across the blade element. Secondary flows are treated in references 26 and 27. Corrections are established in reference 27 for the effect of secondary flows on the outlet angles of compressor inlet guide vanes. At present, however, rotor and stator secondary-flow effects can be treated only on a gross basis.

The effects of changes in axial-velocity ratio on the turning angles of a fixed blade-element geometry are conclusively demonstrated in the rotor investigations of reference 7. There are several origins of varying axial-velocity ratio across a compressor blade element: (1) contraction of the annulus area across the blade row, (2) compressibility, which varies axial-velocity ratio for a fixed annulus area, and (3) differences in the radial gradient of axial velocity at blade-row inlet and outlet, which can arise from the effects of radial-pressure equilibrium (ref. 1). Although several attempts have been made to establish corrections for the effect of change in axial-velocity ratio on deviation angle (refs. 7 and 28), these proposed correction techniques have not been universally successful. The principal difficulty involved in the axial-velocity corrections is the inability to determine the corresponding changes in blade circulation (i.e., tangential velocity). Values of axial-velocity ratio were identified for the deviation angle data presented, although no attempt was made to apply any corrections.

Some of the secondary factors influencing deviation angle, such as inlet Mach number and Reynolds number, are investigated in references 7, 12, and 22. These results indicate that the variations of deviation angle with Mach number and Reynolds number (as in the two-dimensional cascade) are small.

Correlation Approach

In this report, annular-cascade data are compared with the two-dimensional-cascade correlations of minimum loss-incidence angle, total-pressure loss, and deviation angle (ref. 4). In this way, compressor investigations serve as both a verification and an extension of the two-dimensional-cascade data. Two-dimensional-cascade data correlations and rules, in conjunction with correction factors deduced from the three-dimensional data, can then be used for compressor design and analysis.

With this approach in mind, all available single-stage data were collected, computed, and plotted in a form considered convenient for correlation. The blade and performance parameters used in the analysis are similar to those used in the two-dimensional-cascade correlations of reference 4. Camber angle, incidence angle, and deviation angle (fig. 2) are used to define the blade camber, air approach, and air leaving directions, respectively. These angles are based on tangents to blade mean camber line at the leading and trailing edges. As in reference 4, the NACA $65(A_{10})$-series blades are considered in terms of the equivalent circular-arc camber line (figs. 3 and 4).

Loss in total pressure across the blade element is expressed in terms of the loss parameter $\bar{\omega} \cos \beta_2'/2\sigma$, where the relative total-pressure loss coefficient $\bar{\omega}$ is defined as the mass-averaged defect in relative total pressure divided by the pressure equivalent of the inlet velocity head:

$$\bar{\omega} = \frac{P_{2,id}' - P_2'}{P_1' - P_1} \tag{1}$$

(All symbols are defined in appendix A.) For stationary blade rows, or no change in streamline radius across the rotor, the numerator of equation (1) becomes the decrease in relative total pressure across the blade row from inlet to outlet. The relative total-pressure-loss coefficient was computed from stationary measurements of total pressure and total temperature and from the computed relative inlet Mach number according to reference 14. The total-pressure-loss parameter, as indicated in reference 4, approximates the individual blade-wake momentum-thickness ratio θ/c and as such represents a significant parameter for correlating blade losses.

The diffusion factor, which is used as a blade-loading parameter, is defined in reference 14 as follows:[*]

$$D = \left(1 - \frac{V_2'}{V_1'}\right) + \frac{V_{\theta,1}' - V_{\theta,2}'}{2\sigma V_1'} \tag{2}$$

A typical example of the plotted performance parameters for a rotor blade row is shown in figure 5. The data represent the variations of the flow at fixed rotational speed. Plots for stator blade rows show similar trends of variation. As in reference 4, a reference point was established as the incidence angle for minimum loss (fig. 6(a)), and the blade-element flow was analyzed at this reference point. In cases where minimum-loss incidence was not clearly defined, the reference point was taken as the mean incidence of the incidence-angle range for which values of $\overline{\omega}$ at the end points are twice the minimum value (fig. 6(b)).

One of the primary objectives of this analysis is to determine differences in blade-element performance with compressor radial position. Therefore, three radial positions along the blade span (near the hub, mean radius, and tip) of each blade row are considered. The radial positions at the hub and tip are approximately 10 to 15 percent of the passage height away from the inner and outer walls, respectively, which are outside the wall boundary-layer region in all cases. The analysis is directed toward correlating the loss and deviation-angle data at reference incidence angle and determining the variation of reference incidence angle with blade geometry and Mach number at the three radial positions.

---

[*]In a communication to the authors, Dr. Leroy Smith, Jr. of the General Electric Company has suggested that in the presence of a change in radius across a blade element, the diffusion factor for the rotor be given by

$$D_R = \left(1 - \frac{V_2'}{V_1'}\right) + \frac{\Delta(rV_\theta)}{2\sigma_{av} r_{av} V_1'}$$

where r_{av} is the average radius between inlet and outlet, σ_{av} is the corresponding average solidity, and V_θ is the absolute tangential velocity. Other terms are as before. For the stator,

$$D_S = \left(1 - \frac{V_2}{V_1}\right) + \frac{\Delta(rV_\theta)}{2\sigma_{av} r_{av} V_1}$$

Spot checks of hub-position velocity diagrams, where the change in radius is the greatest for the rotors considered, showed small differences between the values of D computed from equation (2) and from these modified relations.

Experimental Data Sources

There are three sources of three-dimensional-cascade blade-element data: stationary annular-cascade tunnel investigations, multistage-compressor investigations, and single-stage or single-blade-row compressor investigations. A relatively small amount of data has been accumulated from blade-row investigations conducted in stationary annular-cascade tunnels. Tunnels of this type have been used primarily for inlet-guide-vane investigations. Typical examples of annular-cascade tunnel investigations are reported in references 18 and 29. Numerous multistage compressor investigations have been conducted both in this country and abroad. Unfortunately, the data obtained from these investigations are too limited to permit the construction of individual blade-row-element performance curves similar to those illustrated in figure 5.

The data used in this investigation were obtained primarily from investigations of single rotor rows or of single-stage compressors. A typical single-stage compressor test installation is shown in figure 7. This particular compressor consists of a row of inlet guide vanes, a rotor blade row driven by a variable-speed motor, and a stator blade row. A discharge throttle is installed in the outlet system to vary the compressor back pressure. In this manner, the compressor mass-flow rate can be controlled. In an installation such as this, compressor performance over a range of speeds and mass flows can be obtained simply. In many cases, test rigs similar to figure 7 have been operated with only guide vanes and rotors or with rotors alone.

Many phases of compressor research have been conducted in single-stage compressor test rigs; and, in reporting these phases, complete blade-element results are not usually presented. Therefore, it was necessary to collect available original data and rework them in terms of the parameters of the analysis. Since only NACA original data were available in blade-element form, the data analysis is based mainly on single-stage compressor investigations conducted at the Lewis laboratory. The measurements taken and the instrumentation used vary somewhat from compressor to compressor; in most cases, however, it is possible from the available data to reconstruct complete experimental velocity diagrams and to determine the blade-element performance. Radial and circumferential survey measurements were made after each blade row. Normally, total pressure, static pressure, total temperature, and air direction were measured. The pressure- and temperature-measuring devices were calibrated for the effect of Mach number.

Most of the compressor investigations that were adaptable to this analysis were conducted on NACA 65-series airfoil shapes and double-circular-arc airfoils. Therefore, the analysis is concerned solely with these airfoils. The 65-series airfoil has been used extensively in subsonic compressors; and the double-circular-arc airfoil, which is a relatively simple airfoil shape, has been used effectively in transonic compressors. Details of the characteristics of the various blade rows used

in this analysis are summarized in table I, and details of the instrumentation, calculation procedure, and accuracy of measurement are given in the listed references.

INCIDENCE-ANGLE ANALYSIS

Method of Correlation

In correlating blade-element reference incidence-angle data, measured values of incidence angle are compared with values of reference incidence angle predicted for the geometry of the blade element according to the low-speed two-dimensional-cascade correlations of reference 4. In reference 4, the low-speed two-dimensional reference incidence angle is expressed in terms of the blade geometry as

$$i_{2-D} = K_i (i_0)_{10} + n\varphi \tag{3}$$

where K_i is a function of blade thickness distribution and maximum thickness ratio, $(i_0)_{10}$ is the zero-camber incidence angle for the 10-percent-thick airfoil section (function of air inlet angle β_1' and solidity σ), and n is equal to $[(i - i_0)/\varphi]_{2-D}$ (also a function of β_1' and σ). Values of K_i, $(i_0)_{10}$, and n for the circular-arc and 65-series blade are repeated in figures 8 to 10 for convenience.

The comparisons between measured blade-element reference incidence angle i_C and predicted two-dimensional incidence angle i_{2-D} are expressed in terms of the difference $(i_C - i_{2-D})$. Thus, a value of zero of the difference parameter corresponds to an equivalence of the two incidence angles. In view of the established tendency of the reference incidence angle to increase somewhat with inlet Mach number (ref. 4), it was thought desirable to plot the variation of the difference parameter $(i_C - i_{2-D})$ against relative inlet Mach number for the three radial positions at hub, mean, and tip.

NACA $65(A_{10})$-series blades. - The results of the comparison between compressor and two-dimensional-cascade reference incidence angle for the NACA $65(A_{10})$-series blades are presented in figure 11 for hub-, mean-, and tip-radius regions. Both rotor and stator data are presented; the stator data being represented by the solid points. Different values of incidence angle for a given symbol represent different compressor tip speeds. As might be expected in a correlation of this type involving data from different test installations and instrumentations, the data are somewhat scattered, particularly in the hub and tip regions. It has

not been possible in these instances to evaluate the significance or origin of the scatter. (In compressor investigations, instrumentation inaccuracy generally contributes heavily to the data scatter, especially at hub and tip.) Nevertheless, the results of the comparison are indicative of the trends involved, and it is possible to make some general observations.

For the rotor mean-radius region, where three-dimensional disturbances are most likely a minimum, the rotor minimum-loss incidence angles are, on the average, about 1^O smaller than the corresponding cascade-predicted values. This difference may be a reflection of some of the compressor influences discussed previously. The data also indicate that no essential variation of reference incidence angle with relative inlet Mach number exists up to values of M_1 of about 0.8. The 65-series blade, having a thick nose profile, apparently exhibits the same approximate constancy of minimum-loss incidence angle with Mach number as indicated for the British thick-nose C4-series profile in the cascade comparisons of reference 4.

At the rotor tip, the compressor reference incidence angles are from 0° to 4° less than the predicted cascade values. As in the case of the rotor mean radius, no essential variation with inlet Mach number is observed in the range of data covered. The lower values of rotor reference incidence angle were generally the result of a change in the form of the variations of loss incidence angle in the rotor, as illustrated in figure 12. The change in form may be explained on the basis of a probable increase in rotor tip three-dimensional losses (centrifuging of blade boundary layer, tip-clearance disturbances, etc.) with increasing incidence angle.

At the rotor hub, the situation is somewhat confused by the wide range of data. A tendency of the compressor incidence angles to be somewhat larger than the corresponding cascade values with an average value of about 1^O or 2^O is indicated.

For the stator mean radius and hub regions, close agreement between compressor and cascade incidence angles is indicated for the range of Mach numbers covered (to about 0.7). Considerable scatter exists in the stator data at the compressor tip; therefore, no definite conclusions can be made concerning the variations of incidence angle.

Double-circular-arc blade. - The results of the double-circular-arc airfoil correlation are presented in figure 13, where compressor reference incidence angle minus low-speed cascade-rule incidence angle (eq. (3)) is plotted against relative inlet Mach number for the hub, mean, and tip radial positions for both rotors and stators. The dashed curve represents the variation obtained with a 25°-camber double-circular-arc blade in high-speed two-dimensional cascade (ref. 4).

It is immediately apparent that rotor reference incidence angle at all radial positions increases with increasing Mach number. The data indicate that the magnitude of the increase in reference incidence angle with Mach number is larger at the hub than at the tip. The hub data points in figure 13 were obtained from blade elements of relatively high camber. Both potential-flow and low-speed cascade results indicate that this type of configuration is associated with a negative value of reference incidence angle. As inlet Mach number is increased, the rate of change of incidence angle in the positive direction must be fairly large in order to avoid high losses associated with blade-row choking, explained in detail in reference 4. In contrast, at the compressor tip, since the blade cambers are generally lower (see table I), the low-speed incidence angle is higher and the required rate of change of incidence angle with increasing Mach number is not as large. Unfortunately, low Mach number data were not available to permit extrapolation of the rotor incidence-angle variations to zero Mach number (level of cascade correlation). However, it is believed that there will be very little change in the rotor incidence angle for values of Mach number below about 0.4 to 0.5. Extrapolated values of rotor reference incidence angle at zero Mach number appear to be of the order of 0.5° at the hub, 1.5° at the mean radius, and 2.5° at the tip below cascade-rule values.

The double-circular-arc blade element in the compressor rotor exhibits the same general incidence-angle characteristic with Mach number that was observed for sharp-nosed blade sections in the high-speed two-dimensional cascade (ref. 4). As indicated in reference 4, the increase in reference incidence angle with Mach number is associated with the tendency of the range of the blade to be reduced only on the low-incidence side of the loss curve as Mach number is increased.

The rotor data for the double-circular-arc section, like those for the 65-series blades, are comparable to the cascade variations at the mean radius, somewhat higher at the hub at the higher Mach numbers, and noticably lower at the tip. Apparently, the same type of three-dimensional phenomenon occurs at the tip for both blade shapes.

The available double-circular-arc stator data are too meager for any conclusions.

Summary Remarks

The variation of reference incidence angle for 65-series and double-circular-arc blade sections has been presented. No Mach number effect on reference incidence angle was observed for the 65-series blades for the range of Mach numbers considered. In contrast, the double-circular-arc blade sections exhibit a pronounced variation of reference incidence angle over the range of Mach number investigated. Significant differences

between the low-speed-cascade data and the rotor data were observed at
the compressor tip. In contrast, at the mean radius and hub, the differ-
ences in two-dimensional-cascade data and rotor data were relatively
small, even though the flow field was three-dimensional.

Additional data are required to determine the variation of stator
reference incidence angle, particularly for the double-circular-arc air-
foil sections. Also, no information has been presented concerning the
allowable incidence-angle range for efficient (low-loss) operation and
the variation of this range with inlet Mach number. Investigations of
these phases of compressor research are very essential to fill gaps in
the compressor design and analysis procedures and warrant attention in
future research programs.

TOTAL-PRESSURE-LOSS ANALYSIS

Correlation of Data

For two-dimensional-cascade data obtained at low Mach numbers, the
values of total-pressure-loss parameter $\bar{\omega} \cos \beta_2'/2\sigma$ plotted against
diffusion factor (eq. (2)) form essentially a single curve for all cas-
cade configurations. The diffusion-factor correlation of loss parameter
was applied to data obtained over a range of Mach numbers from single-
stage axial-flow compressors of various geometries and design Mach num-
bers. Values of total-pressure-loss parameter calculated from single-
stage compressor data are plotted against diffusion factor for the hub,
mean, and tip measuring stations in figure 14. Each symbol represents
the value of diffusion factor and loss parameter at reference incidence
angle at a given tip speed. Also plotted as a dashed curve is the cor-
responding correlation presented in reference 4 for the low-speed two-
dimensional-cascade data. The data of figure 14, which were obtained
from the rotor and stator configurations summarized in table I, represent
both 65-series and circular-arc blade sections. The plots of figure 14
essentially represent an elaboration of the loss-diffusion correlations
of reference 14.

The most important impression obtained from the rotor data plots is
the wide scatter and increasing loss trend with diffusion factor at the
rotor tip, while no discernible trend of variation is obtained at the
rotor hub and mean radii. For the rotor hub and mean radii, it can be
assumed that the rotor blade-element loss parameter follows the cascade
variation but at a higher average magnitude. Unfortunately, the range
of diffusion factor covered in the compressor tests was not sufficient
to determine whether a marked rise in loss is obtained for values of dif-
fusion factor greater than about 0.6 (as in the cascade).

It is apparent from the loss trend and data scatter at the rotor
tip that a different loss phenomenon is occurring in the tip region.   It
is recognized that a part of the scatter is due to the general instrumen-
tation inaccuracy in the highly turbulent tip regions.   In view of the
usually large radial gradients of loss existing in the blade tip region,
small variations in positioning radial survey probes can cause noticeable
differences in the computed results.   Nevertheless, it is obvious that
factors other than the blade-element diffusion are influencing the tip
loss.   The specific three-dimensional factors or origins involved in the
low rise at the tip are not currently known.   The principal conclusion
reached from the plot is that the likelihood of a rising loss trend on
the rotor tip exists for values of diffusion factor greater than about
0.35.

The stator losses at all radial positions in figure 14 appear to be
somewhat higher than those of the two-dimensional cascade, particularly
at the higher values of diffusion factor.

Summary Remarks

Rotor and stator blade-element loss data were correlated by means
of the diffusion factor.   The losses for stator and rotor blade elements
at hub and mean radii were somewhat higher than those for the two-
dimensional cascade over the range of diffusion factor investigated.   At
the rotor tip, the losses were considerably higher at values of diffusion
factor above approximately 0.35.

The foregoing blade-element loss analysis is clearly incomplete.
The need for additional work is indicated for such purposes as evaluating
the origin and magnitude of the tip-region losses.   The loading limits
for rotors at other than the tip region and for stators at all blade ele-
ments have not been determined, because, for the available data, the dif-
fusion factors at reference incidence do not extend to sufficiently high
values.   Single-stage investigations are needed over the critical range of
Reynolds number to determine the effect of Reynolds number on the blade-
element loss.   It is desirable to isolate the effects of velocity diffu-
sion and shock waves on the loss at high Mach number operation.   The loss
correlations presented should also be extended so that the data are ap-
plicable over a range of incidence angle.   This would be of extreme value
in the compressor analysis problem.

DEVIATION-ANGLE ANALYSIS

In addition to design information concerning blade-element losses
and incidence angle, it is, of course, desirable to have a rather com-
plete picture of the air deviation-angle characteristics of axial-flow-
compressor blade elements.   Therefore, the two-dimensional-cascade cor-
relation results are reviewed and supplemented with annular-cascade data
in this section.

Method of Correlation

As in the analysis of reference incidence angle, the correlation of blade-element deviation angle at reference incidence is presented in terms of a comparison between measured blade-element deviation angle and deviation angle predicted for the element according to the low-speed two-dimensional cascade correlations of reference 4. In reference 4, the low-speed two-dimensional deviation angle at reference incidence angle is expressed in terms of blade geometry as

$$\delta^o_{2\text{-}D} = K_\delta (\delta^o_0)_{10} + \frac{m}{\sigma^b} \varphi \tag{4}$$

where K_δ is a function of maximum thickness-chord ratio and thickness distribution, $(\delta^o_0)_{10}$ is the zero-camber deviation angle for the 10-percent-thick airfoil section (function of β'_1 and σ), m is a function of β_1 for the different basic camber distributions, and b is an exponent that is also a function of β'_1.

As was shown previously, the reference incidence angle of the compressor blade element may differ somewhat from the corresponding two-dimensional reference incidence angle. Inasmuch as deviation angle will vary with changing reference incidence angle for a given blade geometry (depending on solidity), the two-dimensional deviation angles were corrected to the reference incidence angles of the compressor blade elements. The corrected deviation angle, as suggested in reference 4, is given by

$$\delta^o_{2\text{-}D} = K_\delta (\delta^o_0)_{10} + \frac{m}{\sigma^b} \varphi + (i_C - i_{2\text{-}D}) \left(\frac{d\delta^o}{di} \right)_{2\text{-}D} \tag{5}$$

where $(d\delta^o/di)_{2\text{-}D}$ is the slope of the two-dimensional variation of deviation angle with incidence angle at reference incidence. Values of K_δ, $(\delta^o_0)_{10}$, m, b, and $(d\delta^o/di)_{2\text{-}D}$ for the circular-arc and $65(A_{10})$-series blade are repeated in figures 15 to 19 for convenience.

Deviation-angle comparisons for the double-circular-arc blade were also made on the basis of Carter's rule for cascade blades (ref. 30):

$$\delta^o_{2\text{-}D} = \frac{m_c}{\sigma^{0.5}} \varphi \tag{6}$$

where m_c is a coefficient that is a function of blade-chord angle (fig. 20).

Carter's rule, which has been used extensively in the design of circular-arc blades, was used as the basis for the more elaborate rule of equation (4). In the calculations, Carter's rule was applied directly to the compressor reference incidence angles.

The comparisons between measured blade-element reference deviation angle δ_C^o and predicted two-dimensional deviation angle δ_{2-D}^o are expressed in terms of the difference parameter $(\delta_C^o - \delta_{2-D}^o)$ against relative inlet Mach number for the three radial positions at hub, tip, and mean radius.

NACA $65(A_{10})$-series blades. - Curves of compressor deviation angle minus cascade-rule deviation angle (eq. (5)) for the 65-series airfoil for both rotors and stators are plotted against relative inlet Mach number for the hub, mean, and tip radial positions in figure 21(a). All values of deviation angle correspond to those at compressor reference incidence angle. As in the case of the incidence-angle and loss correlations, there is considerable scatter of data, particularly in the hub and tip regions. Some of the scatter is believed due to the effects of three-dimensional flows and changes in axial-velocity ratio across the element, but perhaps the most important factors are instrumentation differences and errors. It is generally recognized that it is difficult to measure compressor air angles with an accuracy less than about $\pm 1^o$ to 1.5^o. The correlations must therefore be evaluated on an average or trend basis.

The correlation of rotor data in the mean-radius region is fairly good; axial-velocity ratio varied between about 0.9 to 1.10. On the average, the rotor mean-radius deviation angles are about 0.5^o less than the cascade values. These results agree with previous experience (refs. 7 and 8), which indicated rotor turning angles approximately 1° greater (i.e., deviation angles 1° less) than the two-dimensional-cascade results. If data points for the rotor tip having axial-velocity ratios less than 0.8 are neglected, the average deviation angle is about 0.5^o less than the cascade value. Axial-velocity ratio for the tip-region unflagged data varied between 0.8 and 1.05. For the hub, on the average, the blade-element deviation angles were about 1.0^o greater than the corresponding two-dimensional values. Hub axial-velocity ratios varied between 1.0 and 1.2. As in the two-dimensional cascade (ref. 4), no Mach number effect on deviation angle is indicated over the range of Mach number investigated for all three regions.

For the stator mean-radius $(V_{z,2}/V_{z,1} = 1.0 \text{ to } 1.1)$ and hub-radius $(V_{z,2}/V_{z,1} = 0.85 \text{ to } 1.05)$ regions, the average deviation angles are both about 1.0^o lower than the corresponding two-dimensional values. At the stator tip, the average blade-element value is indicated to be about 4° less than the two-dimensional value. However, these data all have high

axial-velocity ratios (from 1.1 to 1.5). It is expected that, on the
basis of constant axial velocity, the probable average blade-element de-
viation angles at the stator tip might be several degrees closer to the
two-dimensional values. (Increasing axial-velocity ratio at essentially
constant circulation for the stator tends to decrease deviation angle.)
As in the case of the rotor, no essential variation of deviation angle
with Mach number is detected for the stator within the range of Mach num-
bers investigated.

Double-circular-arc blade. - Blade-element and two-dimensional-
cascade deviation angles (eq. (5)) obtained for the double-circular-arc
blade are compared in figure 21(b). The scatter of data is generally
less than for the $65(A_{10})$-series blades, partly because of the generally
more accurate measurements taken in these investigations (all are more
recent than the data of fig. 21(a)).

On the average, at the lower Mach numbers the blade-element deviation
angles were about 1.5° less than the two-dimensional values at the tip,
1.0° greater at the hub, and equal to the two-dimensional values at the
mean region. Ranges of axial-velocity ratio covered for the data were
0.85 to 1.05 at the tip, 0.95 to 1.5 at the hub, and 0.90 to 1.15 at the
mean radius. A slight increasing trend of variation with inlet Mach num-
ber may be indicated at the mean radius and possibly also at the hub.

The double-circular-arc stator data available (solid symbols) are too
limited to permit any reliable conclusions to be drawn. It appears, how-
ever, that at the stator mean radius, the blade-element deviation angles
may be about 0.5° less than the two-dimensional-cascade values. This is
essentially the same trend observed for the $65(A_{10})$-series stators at mean
radius in figure 21(a). Blade-element deviation angles appear to be
greater at the tip and smaller at the hub than the two-dimensional values.
Ranges of axial-velocity ratio were 1.0 to 1.25 at the tip, 0.95 to 1.27
at the mean radius, and 0.9 to 1.30 at the hub.

Blade-element deviation angles and two-dimensional values predicted
by Carter's rule (eq. (6)) are compared in figure 22. Inasmuch as Carter's
rule results in values of two-dimensional deviation angle between 0.5° to
1.0° smaller than obtained from the modified rule of equation (5) for the
range of blade-element geometries included in the data, the agreement with
the blade-element data remains quite good.

Summary Remarks

From the comparisons of measured and predicted reference deviation
angles for the NACA $65(A_{10})$-series and double-circular-arc blades, it
was found that the rules derived from two-dimensional-cascade data can

satisfactorily predict the compressor reference blade-element deviation angle in the rotor and stator mean-radius regions for the blade configurations presented. Larger differences between rule and measured values were observed in the hub and tip regions. These differences can be attributed to the effects of three-dimensional flow, differences in axial-velocity ratio, and measurement inaccuracy. As in the cascade, essentially constant deviation angle with Mach number was indicated for the Mach number range covered. Additional stator blade-element data, particularly for the double-circular-arc blade, are required to establish the stator correlations more firmly.

APPLICATION TO DESIGN

Design Procedure

The foregoing correlations provide a means of establishing the reference incidence angle and estimating the corresponding deviation angle and total-pressure loss for rotor and stator blade elements of compressor designs similar to those covered in the analysis. This is accomplished by establishing deduced curves of compressor blade-element incidence-angle and deviation-angle corrections for the low-speed two-dimensional-cascade rules of reference 4. Reference incidence and deviation angles for the compressor blade element are then given by

$$i_C = i_{2-D} + (i_C - i_{2-D}) \qquad (7)$$

and

$$\delta_C^o = \delta_{2-D}^o + (\delta_C^o - \delta_{2-D}^o) \qquad (8)$$

where i_{2-D} and δ_{2-D}^o are given by equations (3) and by (5) or (6), respectively. Curves of incidence-angle and deviation-angle corrections deduced from the rotor blade-element data of figures 11, 13, 21, and 22 are shown as functions of relative inlet Mach number for several radial positions along the blade height in figures 23 and 24. The curves in figures 23 and 24 are faired average values of the data spread and, strictly speaking, represent bands of values. In view of the very limited data available, compressor correction curves could not reliably be established for the stator deviation and incidence angles.

The establishing of single deduced blade-element loss curves at reference incidence angle is a difficult task because of the scatter of the experimental data, especially in the rotor tip region. Nevertheless, for completeness in order to illustrate the prediction procedures, curves of average total-pressure-loss parameter as a function of diffusion parameter

obtained from the data of figure 14 are shown in figure 25 for rotor and
stator. The shaded portion in the figure indicates the possible band of
values obtainable at the rotor tip.

The procedure involved in determining blade-element camber angle
and efficiency at reference incidence angle for a compressor design based
on the blade-row velocity diagram and the foregoing correlation curves is
now indicated. The desired blade-element turning angle $(\beta_1' - \beta_2')$ and
relative inlet Mach number M_1' are obtained from the design velocity
diagram. Camber and turning angles are related by the equation

$$\varphi = \beta_1' - \beta_2' + \delta^o - i \tag{9}$$

Compressor blade-element incidence (eqs. (3) and (7)) and deviation (eqs.
(5) and (8)) angles are given by

$$i_C = K_i(i_0)_{10} + n\varphi + (i_C - i_{2-D}) \tag{10}$$

$$\delta_C^o = K_\delta(\delta_0^o)_{10} + \frac{m}{\sigma^b}\varphi + (i_C - i_{2-D})\left(\frac{d\delta^o}{di}\right)_{2-D} + (\delta_C^o - \delta_{2-D}^o) \tag{11}$$

Substitution of equations (10) and (11) into equation (9) and rearrange-
ment of terms yield:

$$\varphi = \frac{(\beta_1' - \beta_2') + (\delta_C^o - \delta_{2-D}^o) + (i_C - i_{2-D})\left[\left(\frac{d\delta^o}{di}\right)_{2-D} - 1.0\right] - K_i(i_0)_{10} + K_\delta(\delta_0^o)_{10}}{1 - \frac{m}{\sigma^b} + n}$$

$$\tag{12}$$

All terms on the right side of equation (12) can be determined from
the velocity-diagram properties, the specified blade shape and thickness,
and the specified solidity. After the camber angle is determined, the
incidence and deviation angles can be calculated from equations (10) and
(11). Rotor blade-element loss parameter is estimated from the velocity-
diagram diffusion factor and the curves of figure 14. The total-pressure-
loss coefficient $\bar{\omega}$ is then readily obtained from the blade-element so-
lidity and relative air outlet angle. Blade-element efficiencies for the
rotor and complete stage can be computed by means of the techniques and
equations presented in appendix B. If change in radius across the blade
row can be assumed small, blade-element efficiency can be determined
through the use of figures 26 to 28 from the selected values of $\bar{\omega}$ and
the values of M_1' and absolute total-pressure ratio or total-temperature
ratio obtained from the velocity diagram.

The foregoing procedure can best be illustrated by a numerical example. Suppose the following specified rotor design values represent typical values at 10 percent of the passage height from the compressor tip:

$$\left.\begin{array}{l}\beta_1' = 56.9^\circ \\[2em] \beta_1' - \beta_2' = 10.9^\circ \\[2em] M_1' = 1.1 \\[2em] D = 0.35 \\[2em] \dfrac{T_2}{T_1} = 1.091\end{array}\right\} \text{obtained from velocity-diagram calculations (ref. 1)}$$

$$\left.\begin{array}{l}\sigma = 1.0 \\[2em] t/c = 0.06\end{array}\right\} \text{assumed values}$$

The problem is to find the camber, incidence, and deviation angles and the total-pressure-loss coefficient for a double-circular-arc airfoil section that will establish the velocity-diagram values.

(1) From the value of M_1' and figures 23(b) and 24(b),

$$i_C - i_{2-D} = 4.0^\circ \qquad \delta_C^\circ - \delta_{2-D}^\circ = -1.5^\circ$$

(2) From the values of β_1', σ, and t/c and figures 8 to 10 and 15 to 19,

$$K_i = 0.62 \qquad (i_0)_{10} = 4.4^\circ \qquad n = -0.22 \qquad K_\delta = 0.37$$

$$(\delta_0^\circ)_{10} = 1.6^\circ \qquad m = 0.305 \qquad b = 0.714 \qquad \left(\frac{d\delta^\circ}{di}\right)_{2-D} = 0.1$$

(3) When the values of steps (1) and (2) are substituted in equation (12), the value of blade camber $\varphi = 7.7^\circ$.

(4) From equations (10) and (11), $i_C = 5.0$ and $\delta_C^\circ = 1.8$.

(5) For calculation of the total-pressure-loss coefficient, the diffusion factor (0.35) and figure 25(a) yield a value of (0.025) for the loss parameter $(\bar{\omega} \cos \beta_2')/2\sigma$, and

$$\beta_2' = \beta_1' - (\beta_1' - \beta_2') = 56.9 - 10.9 = 46.0^\circ$$

$$\cos \beta_2' = 0.6947$$

Therefore,

$$\bar{\omega} = \left(\frac{\bar{\omega} \cos \beta_2'}{2\sigma}\right) \frac{2\sigma}{\cos \beta_2'} = \frac{0.025 \times 2}{0.6947} = 0.072$$

(6) For a negligible change in radius across the blade element, the following values can be found from figures 26 and 27:

$$\frac{P_2'}{P_1'} = 0.962 \qquad \eta_{ad} = 0.87 \qquad \frac{P_2}{P_1} = 1.31$$

The preceding example has been carried out for a typical transonic rotor blade section. A similar procedure can be used for stator blade sections when adequate blade-element data become available.

Summary Remarks

The foregoing procedures and data apply only to the reference point (i.e., the point of minimum loss) on the general loss-against-incidence-angle variation for a given blade element. The reference minimum-loss incidence angle, which was established primarily for purposes of analysis, is not necessarily to be considered as a recommended design point for compressor application. The selection of the best incidence angle for a particular blade element in a multistage compressor design is a function of many considerations, such as the location of the blade row, the design Mach number, and the type and application of the design. However, at transonic inlet Mach number levels, the point of minimum loss may very well constitute a desired design setting.

At any rate, the establishment of flow angles and blade geometry at the reference incidence angle can serve as an anchor point for the determination of conditions at other incidence-angle settings. For deviation-angle and loss variations over the complete range of incidence angles, reference can be made to available cascade data. Such low-speed cascade data exist for the NACA $65(A_{10})$-series blades (ref. 31).

It is recognized that many qualifications and limitations exist in the use of the foregoing design procedure and correlation data. For best results, the application of the deduced variations should be restricted to the range of blade geometries (camber, solidity, etc.) and flow conditions (inlet Mach number, Reynolds number, axial-velocity ratio, etc.) considered in the analysis. In some cases for compressor designs with very low turning angle, the calculated camber angle may be negative. For these cases it is recommended that a zero-camber blade section be chosen and the incidence angle selected to satisfy the turning-angle requirements. The data used in the analysis were obtained for the most part from typical experimental inlet stages with essentially uniform inlet flow. Nevertheless, such data have been used successfully in the design of the latter stages of multistage compressors. It should also be remembered that the single curves appearing in the deduced variations represent essentially average or representative values of the experimental data spread. Also, in some cases, particularly for the stator, the available data are rather limited to establish reliable correlations. Considerable work must yet be done to place the design curves on a firmer and wider basis. The design procedures established and trends of variation determined from the data, however, should prove useful in compressor blade-element design.

Lewis Flight Propulsion Laboratory
    National Advisory Committee for Aeronautics
        Cleveland, Ohio, August 9, 1955

APPENDIX A

SYMBOLS

The following symbols are used in this report:

A_{10} 65-series mean-line designation

a_a stagnation velocity of sound, ft/sec

b   exponent in deviation-angle relation (eq. (4)), function of
  inlet-air angle

$C_{L,o}$ isolated-airfoil lift coefficient

c   blade chord, in.

D   diffusion factor, $\left(1 - \dfrac{V'_2}{V'_1}\right) + \dfrac{V'_{\theta,1} - V'_{\theta,2}}{2\sigma V'_1}$, (ref. 14)

i   incidence angle, angle between tangent to blade mean camber line
  at leading edge and inlet-air direction, deg

K_i, K_δ coefficients, functions of blade maximum thickness and thickness
  distribution

M   Mach number

m   coefficient, function of inlet-air angle

m_c coefficient, function of blade-chord angle

n   slope parameter, $\left(\dfrac{i - i_0}{\varphi}\right)_{2-D}$

P   total pressure, lb/sq ft

p   static pressure, lb/sq ft

r   radius

s   blade spacing, in.

T   total temperature

t   blade maximum thickness, in.

V   velocity, ft/sec

β air angle, deg

γ ratio of specific heats

γ^{o} blade-chord angle, deg

δ^{o} deviation angle, angle between tangent to mean camber line at blade trailing edge and air direction, deg

η efficiency

θ momentum thickness, in.

σ solidity, ratio of chord to spacing, c/s

φ camber angle, deg

ω angular velocity, radians/sec

$\bar{\omega}$ total-pressure-loss coefficient

Subscripts:

ad   adiabatic

av   average

C   compressor

GV   inlet guide vanes

h   hub

id   ideal

m   mean

min   minimum

R   rotor

ref   reference

S   stator

ST   stage

t   tip

z   axial direction

θ tangential direction

0   zero camber

1   before blade row or stage

2   after blade row or stage

2-D   low-speed two-dimensional cascade

10   blade maximum thickness-chord ratio of 10 percent

Superscript:

'   relative to rotor

APPENDIX B

EQUATIONS FOR BLADE-ELEMENT EFFICIENCY

By definition, for a complete stage consisting of inlet guide vanes, rotor, and stator, the adiabatic temperature-rise efficiency of the flow along a stream surface is given by

$$\eta_{ST} = \frac{\left(\frac{P_2}{P_1}\right)_{ST}^{\frac{\gamma-1}{\gamma}} - 1}{\left(\frac{T_2}{T_1}\right)_{ST} - 1} = \frac{\left[\left(\frac{P_2}{P_1}\right)_{GV}\left(\frac{P_2}{P_1}\right)_{R}\left(\frac{P_2}{P_1}\right)_{S}\right]^{\frac{\gamma-1}{\gamma}} - 1}{\left(\frac{T_2}{T_1}\right)_{R} - 1} \tag{B1}$$

From the developments of reference 32 (eq. (B8) in the reference), the absolute total-pressure ratio across a blade row P_2/P_1 can be related to the relative total-pressure ratio across the blade row P_2'/P_1' according to the relation

$$\frac{P_2}{P_1} = \frac{\left(\frac{P_2'}{P_1'}\right)}{\left(\frac{P_2'}{P_1'}\right)_{id}}\left(\frac{T_2}{T_1}\right)^{\frac{\gamma}{\gamma-1}} \tag{B2}$$

where $(P_2'/P_1')_{id}$ is the ideal (no loss) relative total-pressure ratio. The relative total pressure is also referred to as the blade-row recovery factor. For stationary blade rows, (i.e., inlet guide vanes and stators), $(P_2'/P_1')_{id}$ is equal to 1.0. For rotors, the ideal relative total-pressure ratio (eq. (B4) of ref. 14) is given by

$$\left(\frac{P_2'}{P_1'}\right)_{id} = \left\{1 + \frac{\gamma-1}{2} M_T^2\left[1 - \left(\frac{r_1}{r_2}\right)^2\right]\right\}^{\frac{\gamma}{\gamma-1}} \tag{B3}$$

in which M_T is equal to the ratio of the outlet element wheel speed to the inlet relative stagnation velocity of sound $(\omega r_2/a_{a,1}')$, and (r_1/r_2)

is the ratio of inlet to outlet radius of the streamline across the blade element. (For a flow at constant radius (cylindrical flow), $(P_2'/P_1')_{id}$ is equal to 1.0.) Thus, from equations (B1) and (B2),

$$\eta_{ST} = \frac{\left[\left(\frac{P_2'}{P_1'}\right)_{GV} \frac{\left(\frac{P_2'}{P_1'}\right)_R}{\left(\frac{P_2'}{P_1'}\right)_{R,id}} - \left(\frac{T_2}{T_1}\right)_R^{\frac{\gamma}{\gamma-1}} \left(\frac{P_2'}{P_1'}\right)_S\right]^{\frac{\gamma-1}{\gamma}} - 1}{\left(\frac{T_2}{T_1}\right)_R - 1} \tag{B4}$$

For the rotor alone, the blade-element efficiency is given by

$$\eta_R = \frac{\left[\frac{\left(\frac{P_2'}{P_1'}\right)_R}{\left(\frac{P_2'}{P_1'}\right)_{R,id}} \left(\frac{T_2}{T_1}\right)^{\frac{\gamma}{\gamma-1}}\right]^{\frac{\gamma-1}{\gamma}} - 1}{\left(\frac{T_2}{T_1}\right)_R - 1} \tag{B5}$$

From equation (B3) of reference 14, the loss coefficient of the rotating blade row (based on inlet dynamic pressure) is given by

$$\bar{\omega}_1' = \left(\frac{P_2'}{P_1'}\right)_{id} \left\{ \frac{1 - \frac{\left(\frac{P_2'}{P_1'}\right)}{\left(\frac{P_2'}{P_1'}\right)_{id}}}{1 - \left[\frac{1}{1 + \frac{\gamma-1}{2}(M_1')^2}\right]^{\frac{\gamma}{\gamma-1}}} \right\} \tag{B6}$$

where $\bar{\omega}_1$ is based on inlet compressible dynamic pressure. For any blade element, then, from equation (B6),

$$\frac{P_2^!}{P_1^!} = \left(\frac{P_2^!}{P_1^!}\right)_{id} - \overline{\omega}_1^! \left\{ 1 - \left[\frac{1}{1 + \frac{\gamma-1}{2}(M_1^!)^2}\right]^{\frac{\gamma}{\gamma-1}} \right\} \qquad (B7)$$

The relations presented in equations (B4), (B5), and (B7) indicate that four quantities are required for the determination of the blade-element efficiency across the rotor or stage: the rotor absolute total-temperature ratio, the relative total-pressure-loss coefficient, (based on inlet dynamic pressure), the relative inlet Mach number, and the ideal relative total-pressure ratio. Thus, the blade-element efficiencies for a given stage velocity diagram can be calculated if the loss coefficients of the blade elements in the various blade rows can be estimated.

For simplicity in the efficiency-estimation procedure, effects of changes in radius across the blade row can be assumed small (i.e., $r_1 = r_2$), so that the ideal relative pressure ratio is equal to unity. Then, equations (B4), (B5), and (B7) become, respectively,

$$\eta_{ST} = \frac{\left[\left(\frac{P_2^!}{P_1^!}\right)_{GV} \left(\frac{P_2^!}{P_1^!}\right)_R \left(\frac{T_2}{T_1}\right)_R^{\frac{\gamma}{\gamma-1}} \left(\frac{P_2^!}{P_1^!}\right)_S\right]^{\frac{\gamma-1}{\gamma}} - 1}{\left(\frac{T_2}{T_1}\right)_R - 1} \qquad (B8)$$

$$\eta_R = \frac{\left[\left(\frac{P_2^!}{P_1^!}\right)_R \left(\frac{T_2}{T_1}\right)_R^{\frac{\gamma}{\gamma-1}}\right]^{\frac{\gamma-1}{\gamma}} - 1}{\left(\frac{T_2}{T_1}\right)_R - 1} \qquad (B9)$$

and

$$\frac{P_2'}{P_1'} = 1 - \overline{\omega}_1' \left\{ 1 - \left[\frac{1}{1 + \frac{\gamma-1}{2} (M_1')^2} \right]^{\frac{\gamma}{\gamma-1}} \right\} \tag{B10}$$

For purposes of rapid calculation and preliminary estimates, the efficiency relations are expressed in chart form in figures 26 to 28. The relation among relative recovery factor, blade-element loss coefficient, and inlet Mach number (eq. (B10)) is presented in figure 26. A chart for determining rotor blade-element efficiency from relative recovery factor and absolute total-temperature ratio (eq. (B9)) is given in figure 27. Lines of constant rotor absolute total-pressure ratio are also included in the figure. Figure 28 presents the ratio of stage efficiency to rotor efficiency for various stator or guide-vane recovery factors. The ratio of stage efficiency to rotor efficiency is obtained from equation (B1) in terms of rotor absolute total-pressure ratio as

$$\frac{\eta_{ST}}{\eta_R} = \frac{\left[\left(\frac{P_2}{P_1}\right)_R \left(\frac{P_2}{P_1}\right)_{GV} \left(\frac{P_2}{P_1}\right)_S \right]^{\frac{\gamma-1}{\gamma}} - 1}{\left(\frac{P_2}{P_1}\right)_R^{\frac{\gamma-1}{\gamma}} - 1} \tag{B11}$$

The charts are used as follows: For known or estimated values of rotor total-pressure-loss coefficient $\overline{\omega}_1'$ and relative inlet Mach number of the element M_1', the corresponding value of relative recovery factor P_2'/P_1' is determined from figure 26. From the value of rotor-element absolute total-temperature ratio T_2/T_1 (obtained from calculations of the design velocity diagram) and the value of (P_2'/P_1') obtained from figure 26, the rotor element efficiency is determined from figure 27. Rotor absolute total-pressure ratio can also be determined from the dashed lines in figure 27.

If inlet guide vanes and stators are present, the respective recovery factors of each blade row are first obtained from figure 26. The product of the two recovery factors is then calculated and used in conjunction with the rotor absolute total-pressure ratio in figure 28 to determine the ratio of stage efficiency to rotor efficiency. A simple multiplication then yields the magnitude of the stage efficiency along the element stream surface.

The charts can also be used to determine gross or mass-averaged efficiencies through the use of over-all loss terms. Furthermore, the charts can be used for the rapid determination of relative total-pressure-loss coefficient from known values of efficiency, pressure ratio, and inlet Mach number on an element or gross basis.

REFERENCES

1. Giamati, Charles C., Jr., and Finger, Harold B.: Aerodynamic Design of Axial-Flow Compressors. VIII - Design Velocity Distribution in Meridional Plane. NACA RM

2. Robbins, William H., and Dugan, James F., Jr.: Aerodynamic Design of Axial-Flow Compressors. X - Prediction of Off-Design Performance of Multistage Compressors. NACA RM E55D05.

3. Roudebush, William H.: Aerodynamic Design of Axial-Flow Compressors. IV - Potential Flow in Two-Dimensional Cascades. NACA RM E54H26.

4. Lieblein, Seymour: Aerodynamic Design of Axial-Flow Compressors. VI - Experimental Flow in Two-Dimensional Cascades. NACA RM

5. Bowen, John T., Sabersky, Rolf H., and Rannie, W. Duncan: Theoretical and Experimental Investigations of Axial Flow Compressors, Pt. 2. Mech. Eng. Lab., C.I.T., July 1949. (Navy Contract N6-ORI-102, Task Order IV.)

6. Alsworth, Charles C., and Iura, Toru: Theoretical and Experimental Investigations of Axial Flow Compressors. Pt. 3 - Progress Report on Loss Measurements in Vortex Blading. Mech. Eng. Lab., C.I.T., July 1951. (Navy Contract N6-ORI-102, Task Order IV.)

7. Schulze, Wallace M., Erwin, John R., and Ashby, George C., Jr.: NACA 65-Series Compressor Rotor Performance with Varying Annulus-Area Ratio, Solidity, Blade Angle, and Reynolds Number and Comparison with Cascade Results. NACA RM L52L17, 1953.

8. Ashby, George C., Jr.: Comparison of Low-Speed Rotor and Cascade Performance for Medium-Camber NACA 65-$(C_{l_o}A_{10})$10 Compressor-Blade Sections over a Wide Range of Rotor Blade-Setting Angles at Solidities of 1.0 and 0.5. NACA RM L54I13, 1954.

9. Andrews, S. J., and Ogden, H.: A Detailed Experimental Comparison of Blades Designed for Free Vortex Flow and Equivalent Untwisted Constant Section Blades. Rep. No. R.123, British N.G.T.E., Aug. 1952.

10. Bullock, Robert O., Johnsen, Irving A., and Lieblein, Seymour: Aero-
      dynamic Design of Axial-Flow Compressors. III - Compressor Design
      System. NACA RM

11. Lieblein, Seymour: Review of High-Performance Axial-Flow-Compressor
      Blade-Element Theory. NACA RM E53L22, 1954.

12. Savage, Melvyn, Erwin, John R., and Whitney, Robert P.: Investigation
      of an Axial-Flow Compressor Rotor Having NACA High-Speed Blade Sec-
      tions (A_2I_{8b} Series) at Mean Radius Relative Inlet Mach Numbers up
      to 1.13. NACA RM L53G02, 1953.

13. Schwenk, Francis C., Lieblein, Seymour, and Lewis, George W., Jr.:
      Experimental Investigation of an Axial-Flow Compressor Inlet Stage
      Operating at Transonic Relative Inlet Mach Numbers. III - Blade-
      Row Performance of Stage with Transonic Rotor and Subsonic Stator
      at Corrected Tip Speeds of 800 and 1000 Feet Per Second. NACA RM
      E53G17, 1953.

14. Lieblein, Seymour, Schwenk, Francis C., and Broderick, Robert L.:
      Diffusion Factor for Estimating Losses and Limiting Blade Loadings
      in Axial-Flow-Compressor Blade Elements. NACA RM E53D01, 1953.

15. Savage, Melvyn: Analysis of Aerodynamic Blade-Loading-Limit Param-
      eters for NACA 65-$(C_{l_o}A_{10})$10 Compressor-Blade Sections at Low Speeds.
      NACA RM L54L02a, 1955.

16. Moses, Jason J., and Serovy, George K.: Effect of Blade-Surface
      Finish on Performance of a Single-Stage Axial-Flow Compressor.
      NACA RM E51C09, 1951.

17. Moses, J. J., and Serovy, G. K.: Some Effects of Blade Trailing-Edge
      Thickness on Performance of a Single-Stage Axial-Flow Compressor.
      NACA RM E51F28, 1951.

18. Thurston, Sidney, and Brunk, Ralph E.: Performance of a Cascade in
      an Annular Vortex-Generating Tunnel over a Range of Reynolds Num-
      bers. NACA RM E51G30, 1951.

19. Wallner, Lewis E., and Fleming, William A.: Reynolds Number Effect
      on Axial-Flow Compressor Performance. NACA RM E9G11, 1949.

20. Mühlemann, E. (John Perl, trans.): Experimental Investigations on
      an Axial Blower Stage. Lockheed Aircraft Corp., Burbank (Calif.).

21. Roudebush, William H., and Lieblein, Seymour: Aerodynamic Design of
      Axial-Flow Compressors. V - Viscous Flow in Two-Dimensional Cas-
      cades. NACA RM

22. Dugan, Paul D., Mahoney, John J., and Benser, William A.: Effect of
    Mach Number on Performance of an Axial-Flow Compressor Rotor-Blade
    Row. NACA RM E8D29, 1948.

23. Voit, Charles H., Guentert, Donald C., and Dugan, James F.: Effect
    of Mach Numbers on Over-All Performance of Single-Stage Axial-Flow
    Compressor Designed for High Pressure Ratio. NACA RM E50D26, 1950.

24. Robbins, William H., and Glaser, Frederick W.: Investigation of an
    Axial-Flow Compressor Rotor with Circular-Arc Blades Operating up
    to a Rotor-Inlet Relative Mach Number of 1.22. NACA RM E53D24,
    1953.

25. Herzig, Howard Z., and Hansen, Arthur G.: Aerodynamic Design of
    Axial-Flow Compressors. XIV - Three-Dimensional Compressor Flow
    Theory and Real Flow Effects. NACA RM E55D04a.

26. Hansen, Arthur G., and Herzig, Howard Z.: Aerodynamic Design of
    Axial-Flow Compressors. XV - Secondary Flows and Three-Dimensional
    Boundary-Layer Effects. NACA RM E55D06.

27. Lieblein, Seymour, and Ackley, Richard H.: Secondary Flows in Annu-
    lar Cascades and Effects on Flow in Inlet Guide Vanes. NACA RM
    E51G27, 1951.

28. Erwin, John R., and Emery, James C.: Effect of Tunnel Configuration
    and Testing Technique on Cascade Performance. NACA Rep. 1016, 1951.
    (Supersedes NACA TN 2028.)

29. Mankuta, Harry, and Guentert, Donald C.: Some Effects of Solidity on
    Turning Through Constant-Thickness Circular-Arc Guide Vanes in Axial
    Annular Flow. NACA RM E51E07, 1951.

30. Carter, A. D. S., and Hughes, Hazel P.: A Theoretical Investigation
    into the Effect of Profile Shape on the Performance of Airfoils
    in Cascade. R. & M. No. 2384, British A.R.C., Mar. 1946.

31. Felix, A. Richard: Summary of 65-Series Compressor-Blade Low-Speed
    Cascade Data by Use of the Carpet-Plotting Technique. NACA RM
    L54H18a, 1954.

32. Howell, A. R.: Design of Axial Flow Compressors. War Emergency
    Issue No. 12 pub. by Inst. Mech. Eng. (London), 1945. (Reprinted
    in U. S. by A.S.M.E., Jan. 1947, pp. 452-462.)

33. Jackson, Robert J.: Effects on the Weight-Flow Range and Efficiency
    of a Typical Axial-Flow Compressor Inlet Stage That Result from the
    Use of a Decreased Blade Camber or Decreased Guide-Vane Turning.
    NACA RM E52G02, 1952.

34. Jackson, Robert J.:   Analysis of Performance of Four Symmetrical-
     Diagram-Type Subsonic Inlet-Stage Axial-Flow Compressors. NACA
     RM E53K03, 1954.

35. Mahoney, John J., Dugan, Paul D., Budinger, Raymond E., and Goelzer,
     H. Fred : Investigation of Blade-Row Flow Distributions in Axial-
     Flow-Compressor Stage Consisting of Guide Vanes and Rotor-Blade
     Row. NACA RM E50G12, 1950.

36. Standahar, Raymond M., and Serovy, George K.: Some Effects of Chang-
     ing Solidity by Varying the Number of Blades on Performance of an
     Axial-Flow Compressor Stage. NACA RM E52A31, 1952.

37. Serovy, George K., Robbins, William H., and Glazer, Frederick W.:
     Experimental Investigation of a 0.4 Hub-Tip Diameter Ratio Axial-
     Flow Compressor Inlet Stage at Transonic Inlet Relative Mach Num-
     bers. I - Rotor Design and Over-All Performance at Tip Speeds
     from 60 to 100 Percent of Design. NACA RM E53I11, 1953.

38. Tysl, Edward R., Schwenk, Francis C., and Watkins, Thomas B.: Experi-
     mental Investigation of a Transonic Compressor Rotor with a 1.5-Inch
     Chord Length and an Aspect Ratio of 3.0. I - Design, Over-All Per-
     formance, and Rotating-Stall Characteristics. NACA RM E54L31, 1955.

39. Lewis, George W., Jr., Schwenk, Francis C., and Serovy, George K.:
     Experimental Investigation of a Transonic Axial-Flow-Compressor
     Rotor with Double-Circular-Arc Airfoil Blade Sections. I - Design,
     Over-All Performance, and Stall Characteristics. NACA RM E53L21a,
     1954.

40. Sandercock, Donald M., Lieblein, Seymour, and Schwenk, Francis C.:
     Experimental Investigation of an Axial-Flow Compressor Inlet Stage
     Operating at Transonic Relative Inlet Mach Numbers. IV - Stage and
     Blade-Row Performance of Stage with Axial-Discharge Stators. NACA
     RM E54C26, 1954.

TABLE I. - DETAILS OF SINGLE-STAGE ROTORS AND STATORS

Blade row	Description	Outer diameter, in.	Hub-tip ratio	Rotor tip speed, ft/sec	Inlet Mach number, M_1	Camber angle, φ, deg		Chord, c, in.		Solidity, σ		Blade chord angle, γ, deg		Blade maximum thickness chord ratio, t/c		References
						Hub	Tip	Hub	Tip	Hub	Tip	Hub	Tip	Hub	Tip	
65-Series blade section																
1	Rotor	14	0.5	552,828,994 1104,1214	0.30-0.75	19.9	15.3	1.31	1.31	1.010	0.590	30.8	56.4	10	10	33
2	Stator	14	.55	552,1104	.26- .73	30.1	30.1	1.31	1.31	.996	.620	19.5	45.9	10	10	34
3	Rotor	30	.80	504,672,840	.36- .70	30.1	30.1	2.90	2.90	1.08	.906	28.8	45.9	10	10	35
4	Rotor	14	.50	1104,1214	.60- .80	30.1	30.1	1.31	1.31	1.010	.590	21.1	56.0	10	10	34
5	Rotor	14	.50	557,743	.39- .72	30.1	30.1	1.31	1.31	.962	.608	15.2	32.0	10	10	34
6	Stator	14	.52	391,557,743	.22- .66	30.1	30.1	1.31	1.31	.993	.631	16.2	32.2	10	10	34
7	Rotor	14	.50	546	.35- .56	40.0	23.9	1.31	1.31	.955	.600	21.0	58.0	10	10	33
8	Rotor	14	.50	552,1104,828	.30- .86	40.0	23.9	1.31	1.31	.955	.600	21.0	58.0	10	10	33
9	Rotor	14	.50	552,828,1104 1214	.30- .76	40.0	23.9	1.31	1.31	.955	.600	21.0	58.0	10	10	33
10	Stator	14	.53	412,617,823	.25- .74	30.1	30.1	1.31	1.31	.970	.587	15.1	39.6	10	10	34
11	Rotor	14	.80	669,753,836	.52- .75	45.2	34.1	1.35	1.35	.823	.692	21.4	35.4	6	6	36
12	Rotor	14	.80	669,753,836	.49- .75	45.2	34.1	1.35	1.35	1.12	.943	21.4	35.4	6	6	36
13	Rotor	14	.80	669,753,836	.49- .75	45.2	34.1	1.35	1.35	1.69	1.35	21.4	35.4	6	6	36
14	Rotor	14	.80	600,736,874	.50- .92	30.3	19.4	1.46	1.82	1.20	1.20	42.5	48.8	10	8	17
Circular-arc blade section																
15	Rotor	14	0.4	600,800,1000	0.33-1.06	40.3	11.4	2.00	2.00	1.778	0.963	12.1	46.7	8	5	37
16	Rotor	18.0	.5	600,700,800 900,1000	.38-1.07	28.3	7	1.5	1.5	1.63	1.03	23.6	46.3	10	6	38
17	Rotor	14	.5	600,800,900 1000	.37-1.17	29.4	13.7	2.09	2.32	1.28	1.04	23.0	44.1	8	5	39
18	Rotor	14	.5	800,900	.55-1.12	29.4	13.7	2.09	2.32	.85	.66	23.0	44.1	8	5	39
19	Rotor	14	.5	800,900,1000 1120	.50-1.22	23.1	4.3	1.50	1.50	1.40	.825	17.4	51.3	10	5	24
20	Rotor	14	.5	800,900,1000 1120	.4 - .82	23.1	4.3	1.50	1.50	1.40	.825	17.4	51.3	10	5	24
21	Stator	17.36	.62	600,800,900	.41- .63	52.0	52.0	3.25	3.25	1.64	1.07	10.0	10.0	7	7	40
22	Stator	17.36	.60	800,1000	.53- .66	20.6	20.0	2.66	3.23	1.45	1.08	34.0	28.0	8	6	13

Compressor axis

Compressor
blade elements

r_t

r_m

r_h

CD-4360
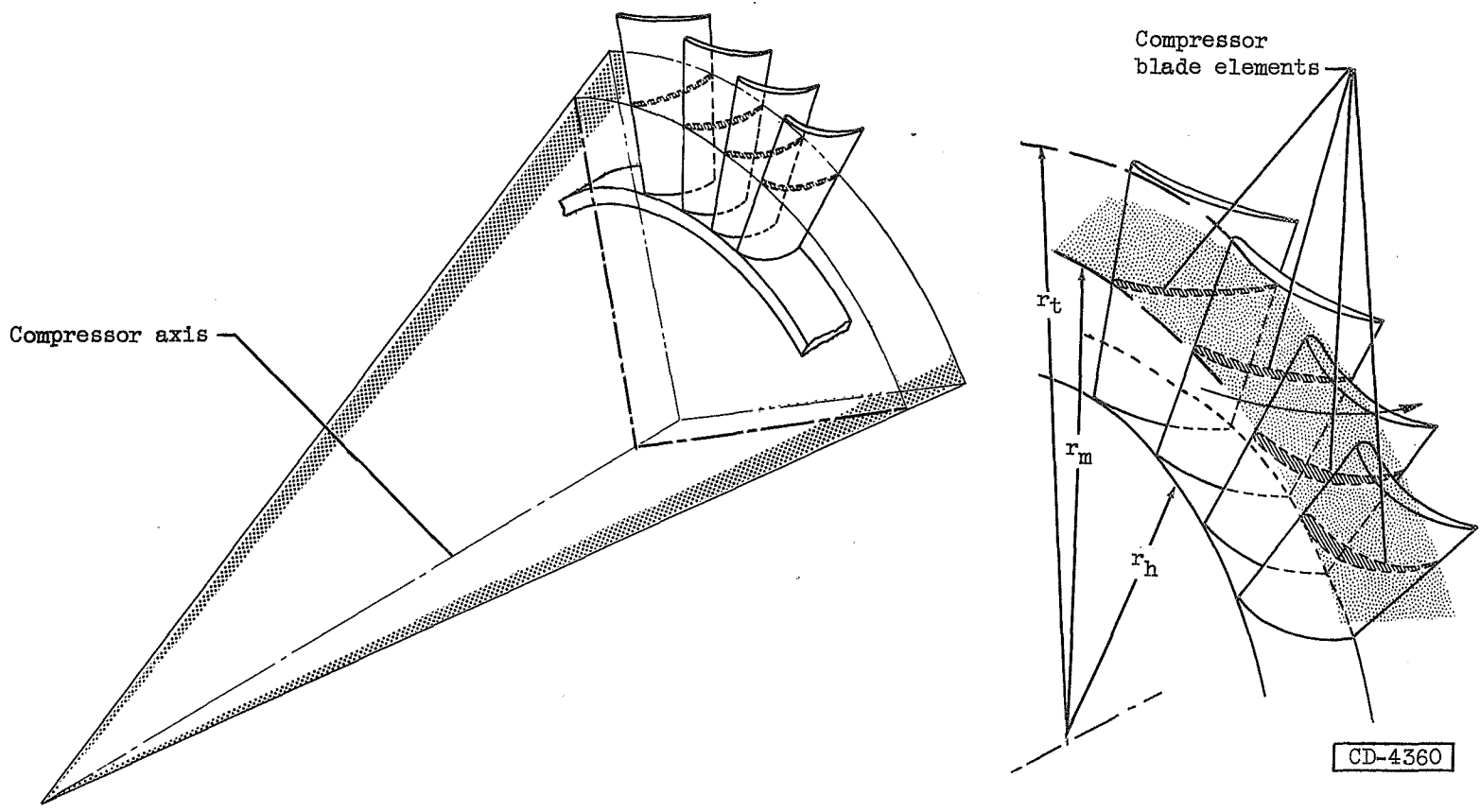
Figure 1. - Compressor blade elements shown along conical surface of revolution
about compressor axis.
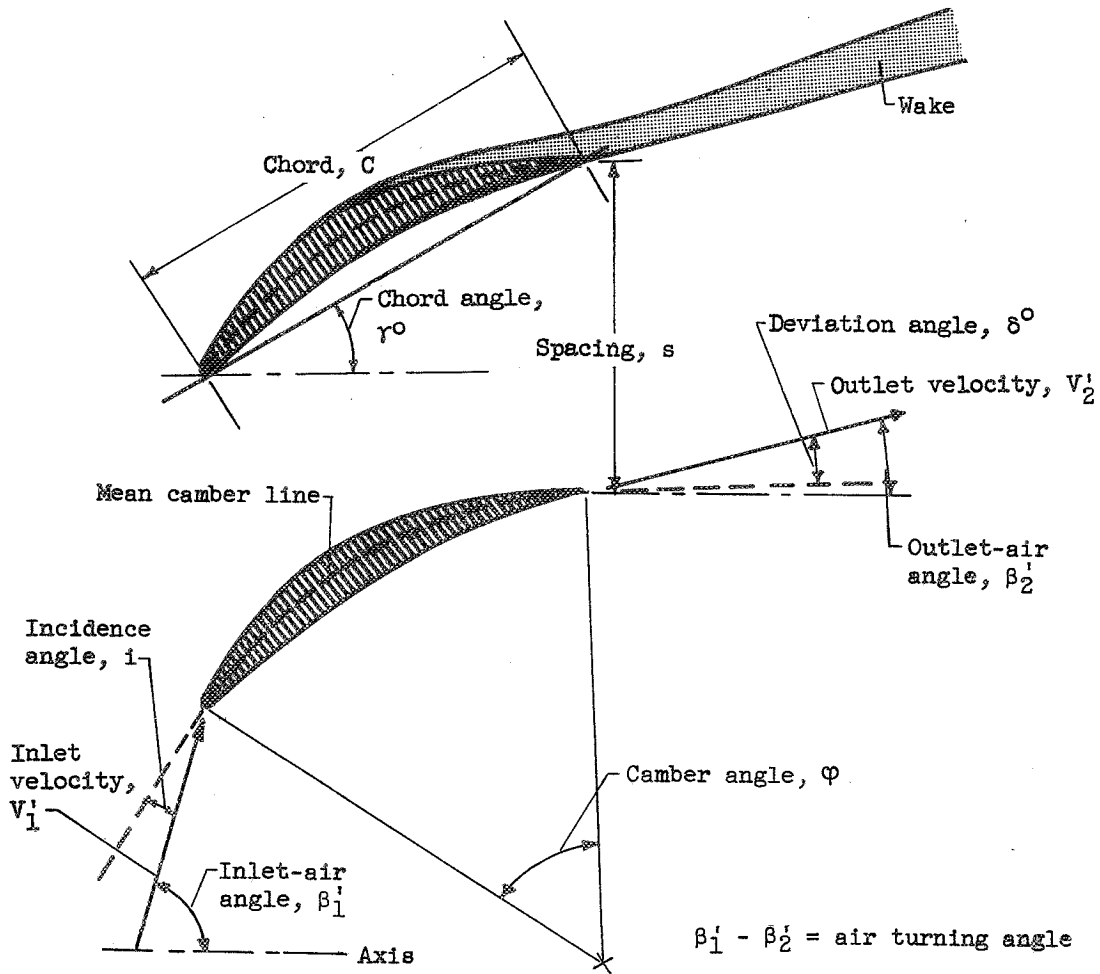
Figure 2. - Blade-element properties.
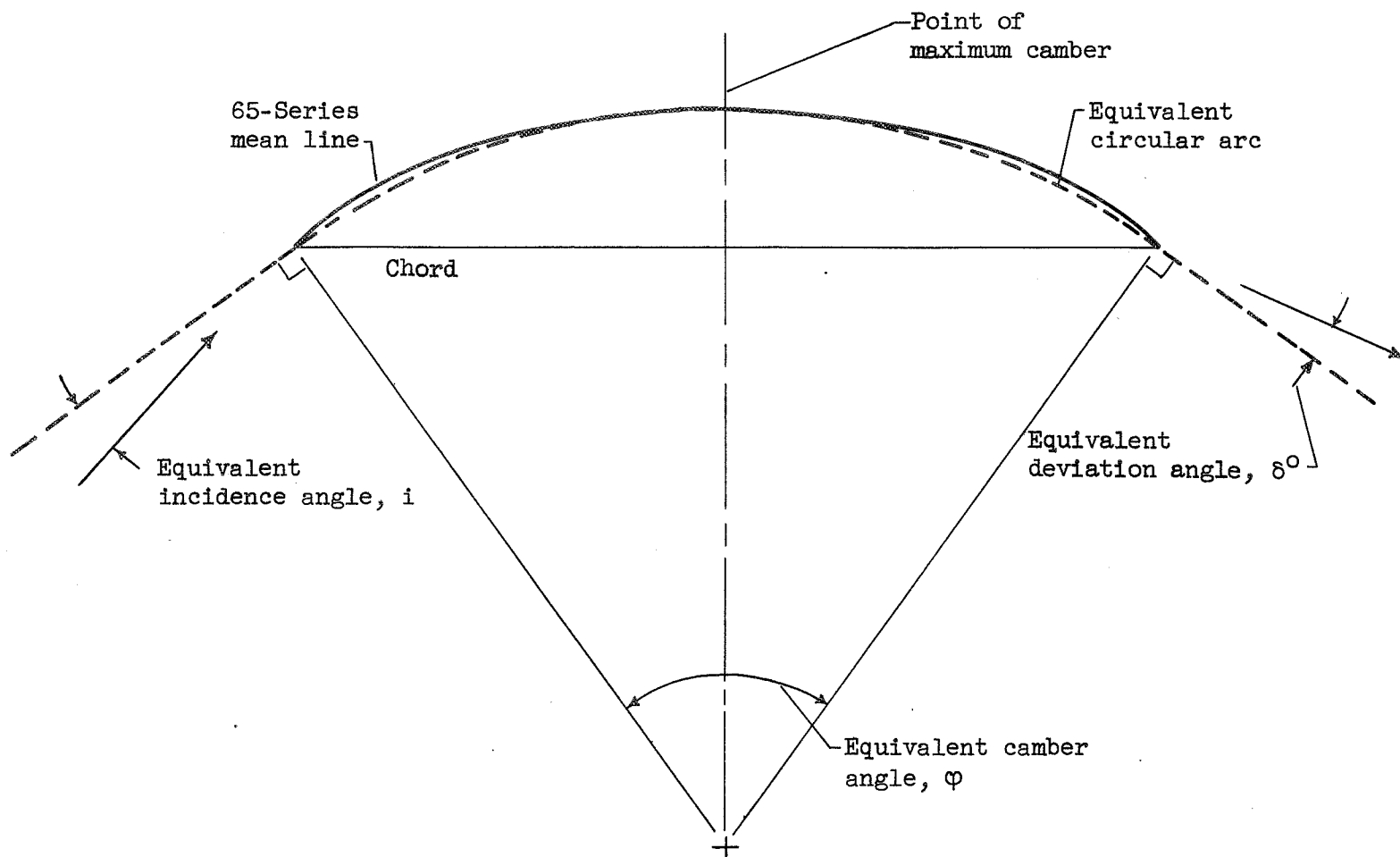
Figure 3. - Equivalent circular-arc mean line for NACA $65(A_{10})$-series blades.
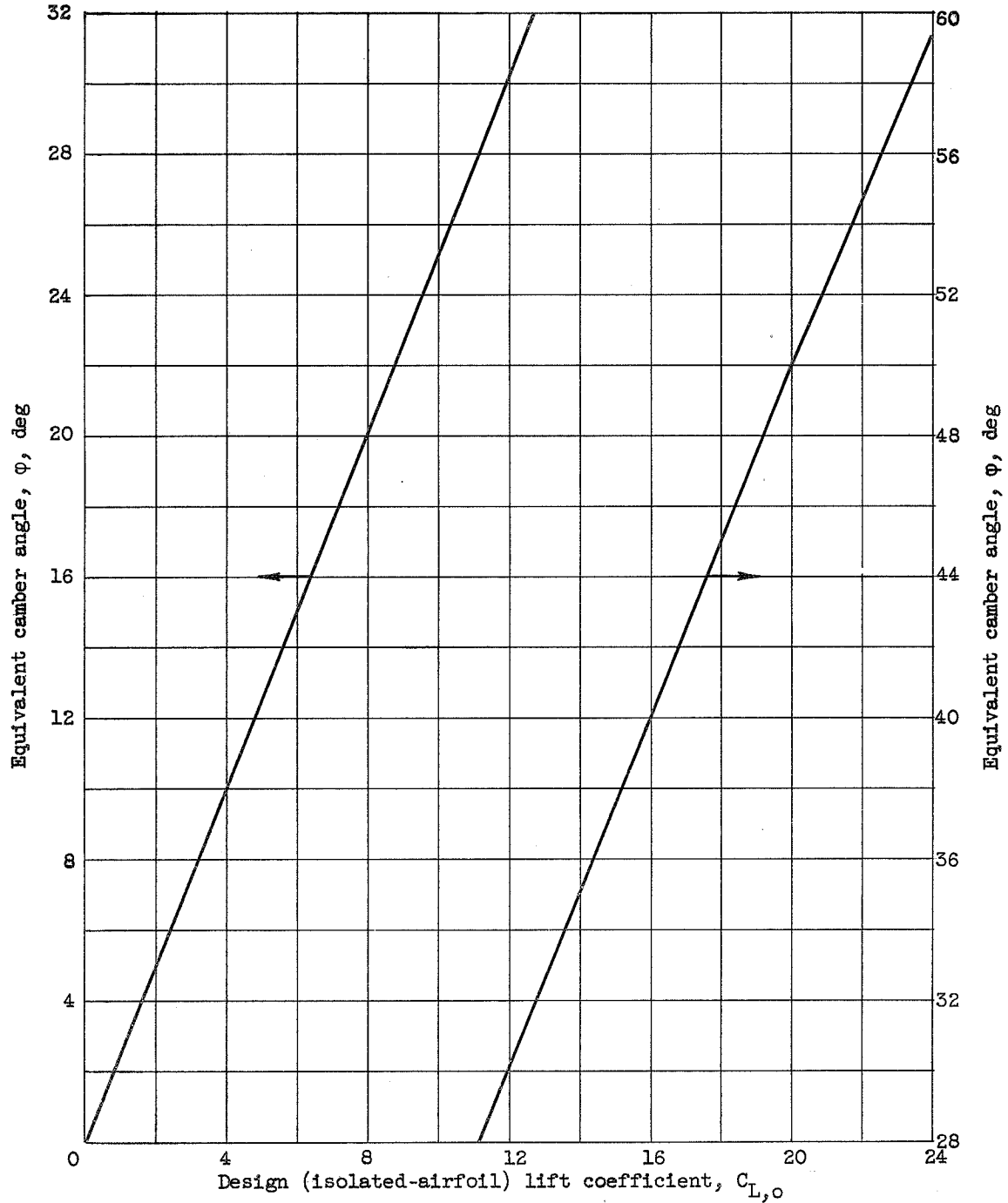
Figure 4. - Equivalent camber angles for NACA $65(C_{l_o}A_{10})$ mean camber line as equivalent circular arc (fig. 3).
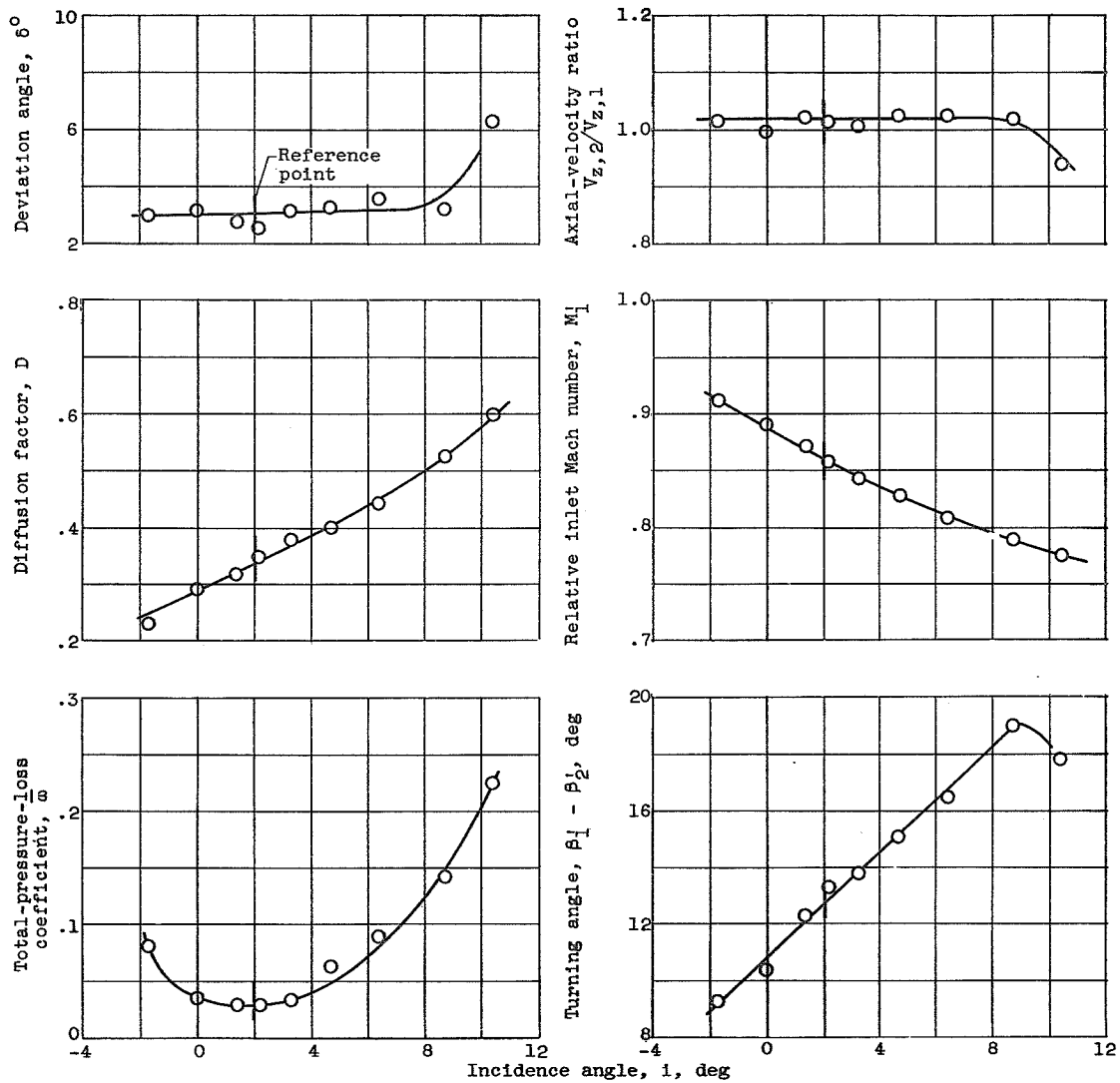
Figure 5. – Examples of typical variation of blade-element performance parameters with incidence angle. Transonic rotor with double-circular-arc blade sections at tip speed of 800 feet per second; data for blade row 17 (table I) at tip position (ref. 39).
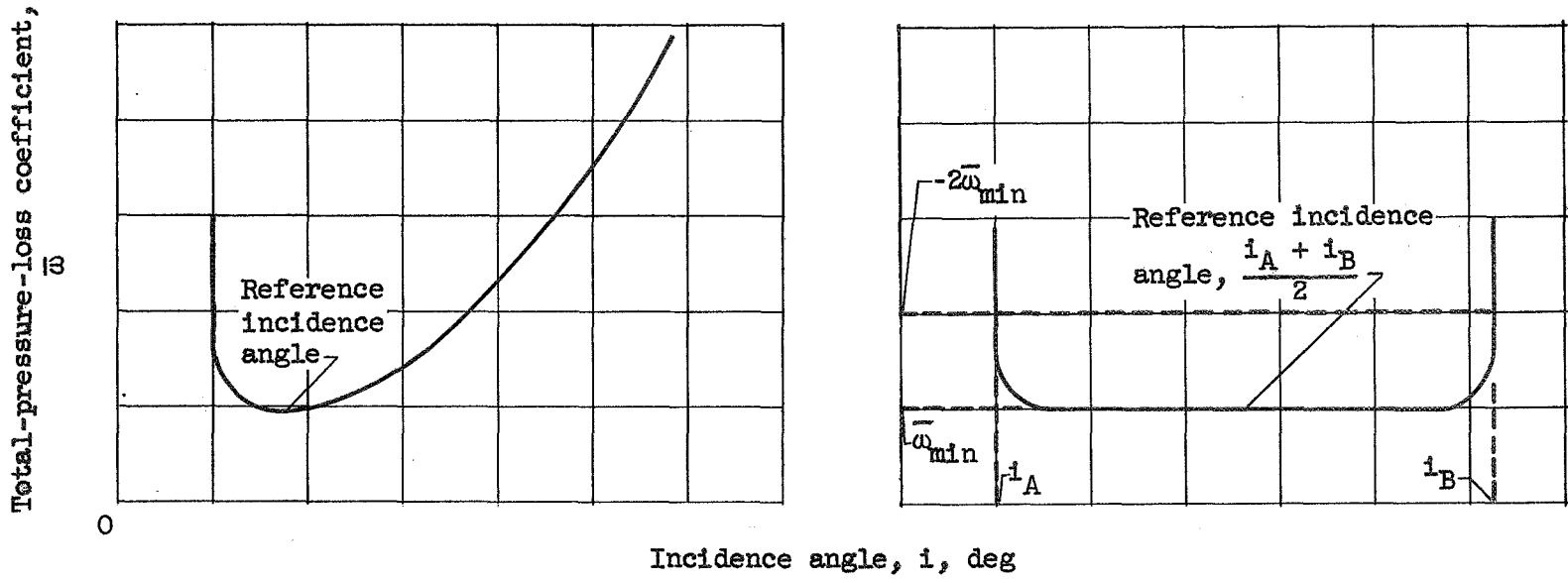
(a) Minimum-loss.

(b) Mid-range.

Figure 6. - Definitions of reference incidence angle.

Orifice tank

Inlet throttle

Thin-plate orifice

High-speed dynamometer

Collector

Stator blades

Rotor blades

Guide vanes

Outlet throttle

Filter, screens, and honeycomb

Depression tank
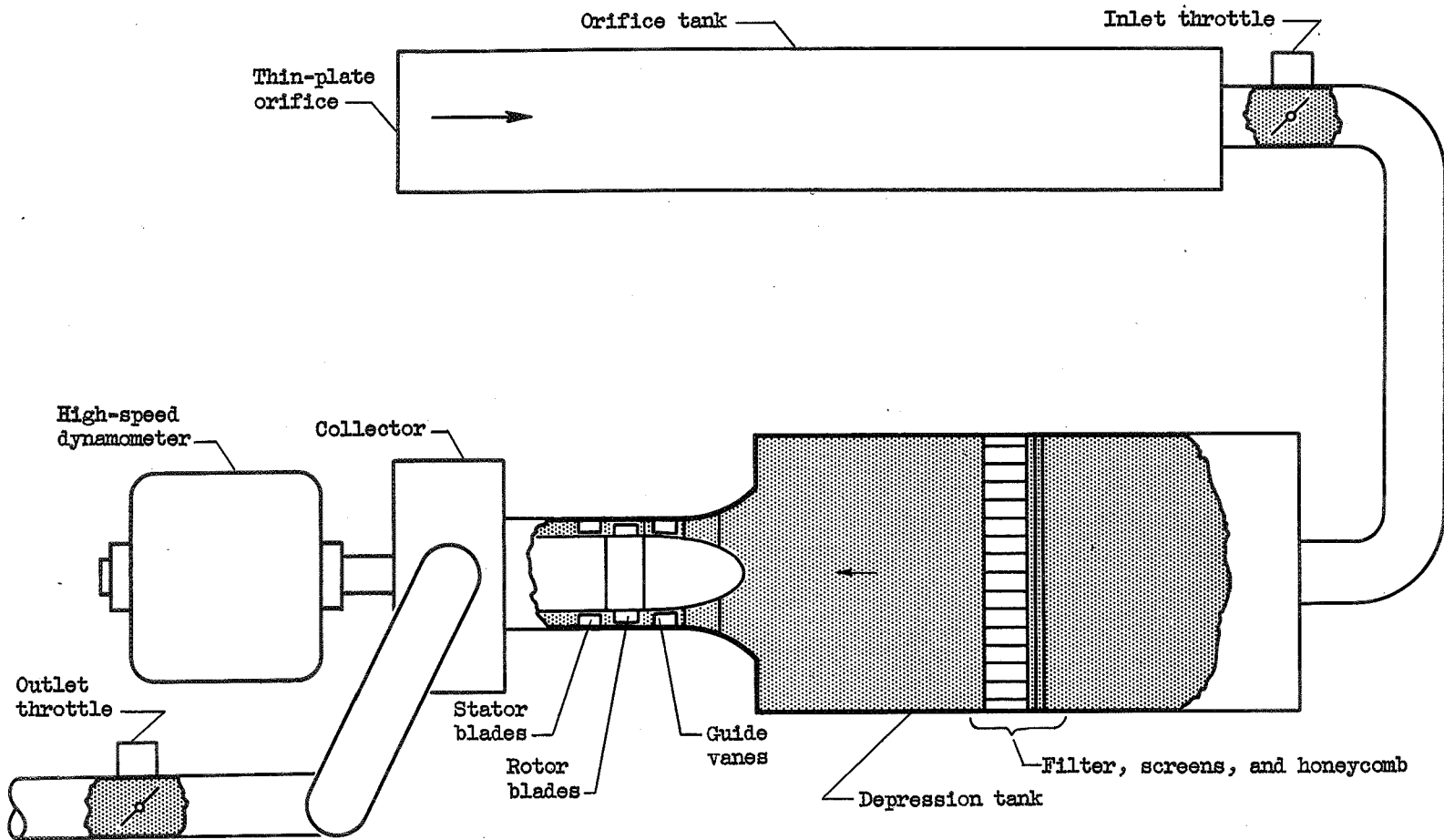
CD-1714

Figure 7. - Schematic diagram of single-stage compressor test installation.
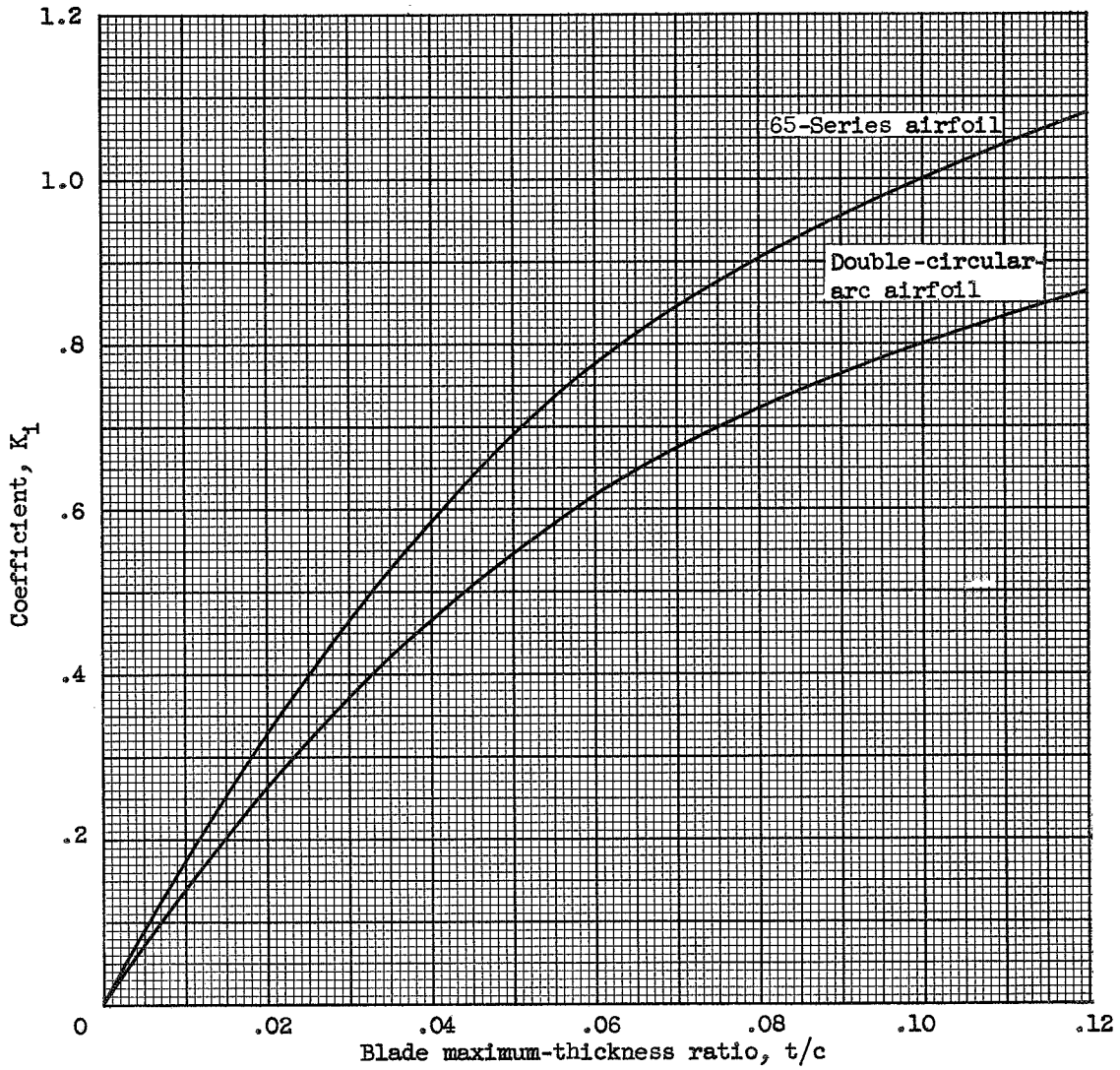
Figure 8. - Thickness correction for zero-camber reference incidence angle (ref. 4).
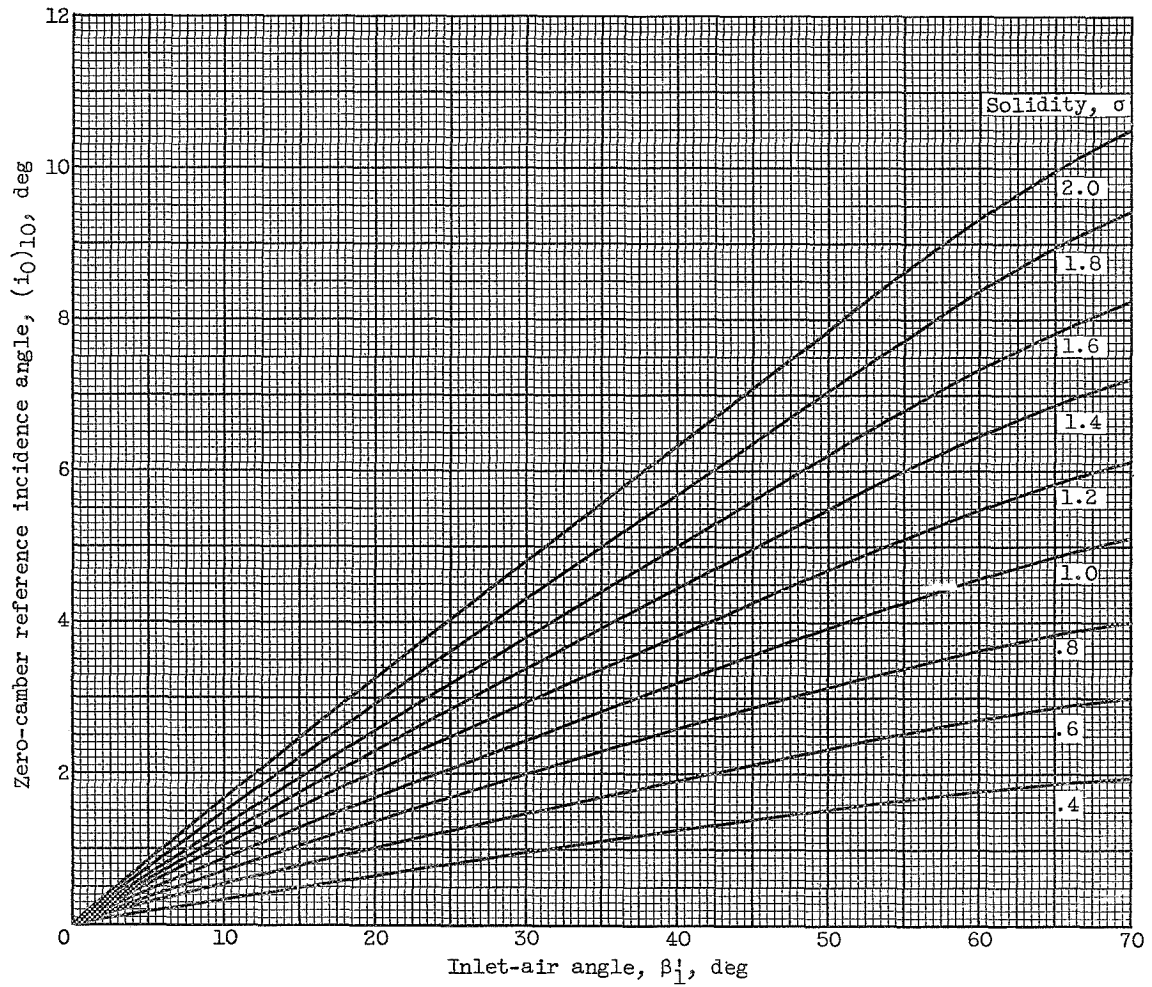
Figure 9. - Zero-camber reference incidence angle for NACA 65-series and true circular-arc blades of 10-percent thickness ratio (ref. 4).
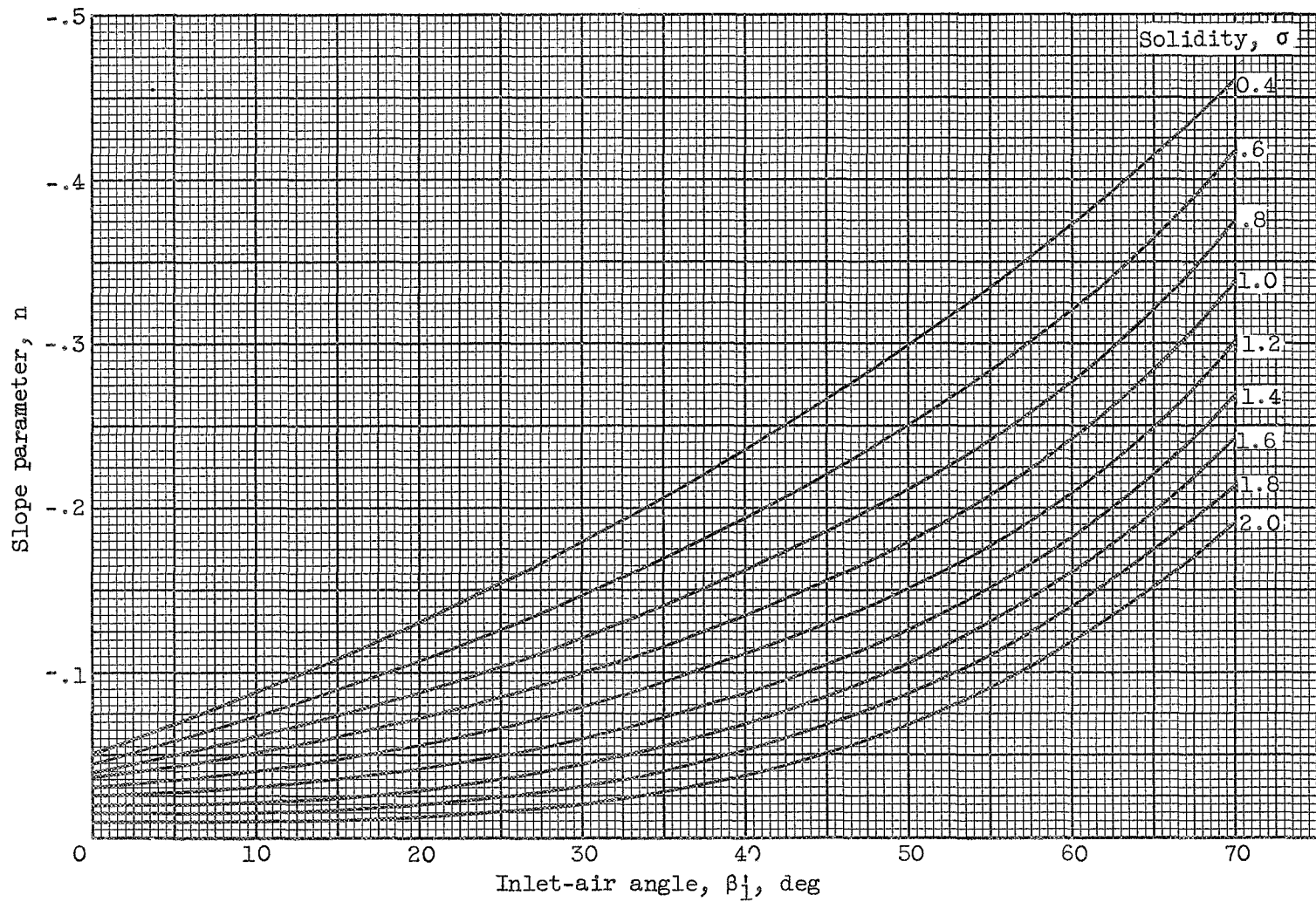
Figure 10. - Reference-incidence-angle slope parameter for NACA 65-series blades as equivalent circular arcs and for true circular-arc blades (ref. 4).
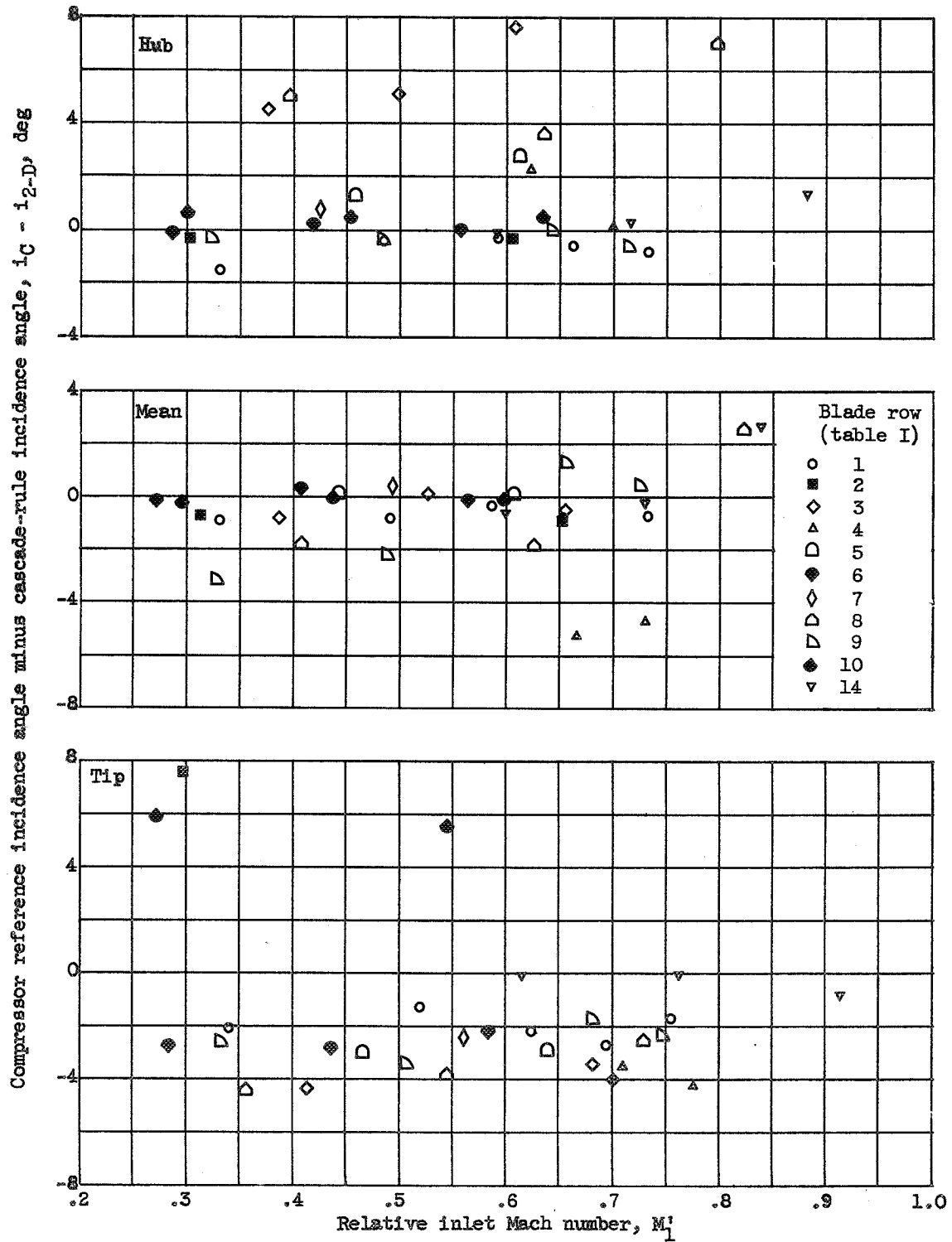
Figure 11. - Variation of compressor reference incidence angle minus two-
    dimensional-cascade-rule incidence angle with relative inlet Mach number
    for NACA 65-series blade section.
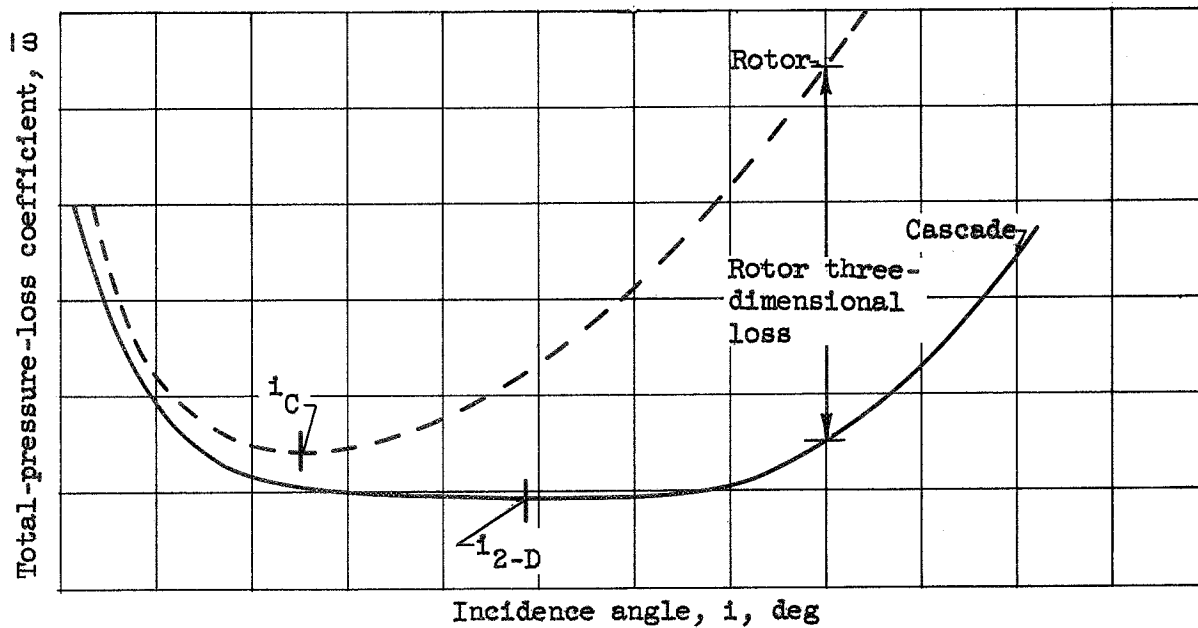
Figure 12. - Typical variation of loss with incidence angle for rotor blade element near tip and in two-dimensional cascade for same blade geometry and inlet Mach number.
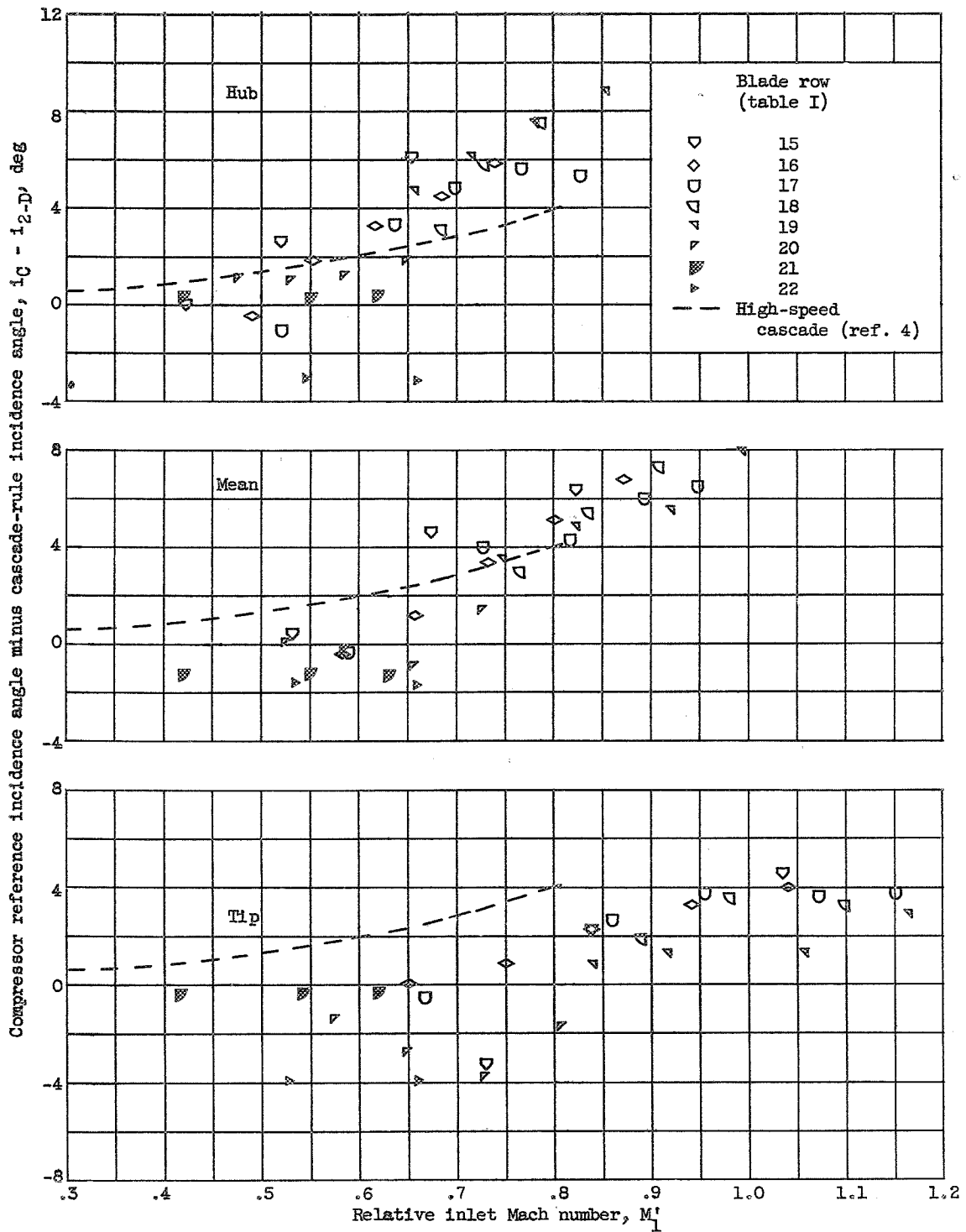
Figure 13. - Variation of compressor reference incidence angle minus two-dimensional-cascade-rule incidence angle with relative inlet Mach number for double-circular-arc blade section.
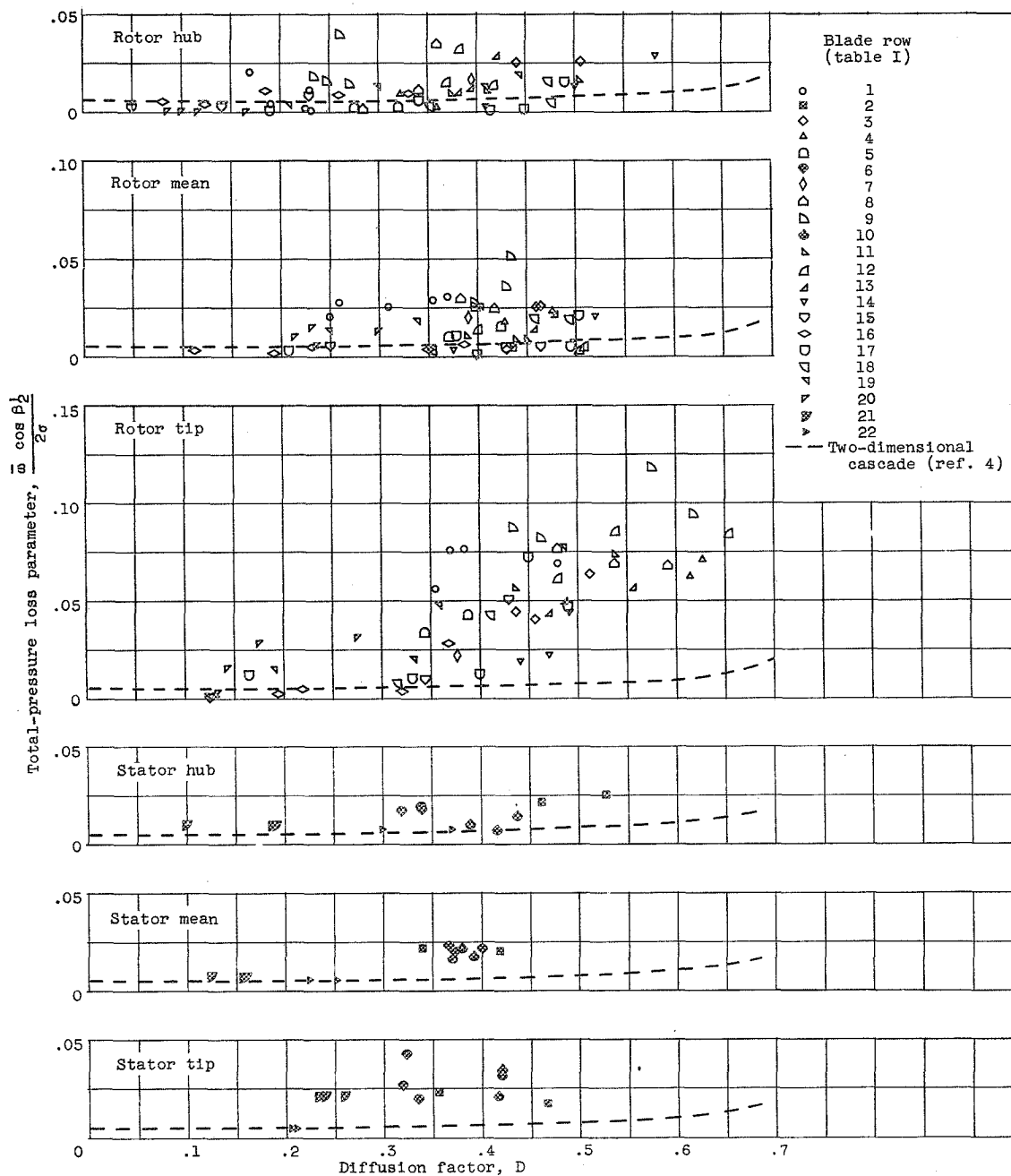
Figure 14. - Variation of total-pressure loss parameter with diffusion factor at reference incidence angle for NACA $65(A_{10})$-series and double-circular-arc blade sections.
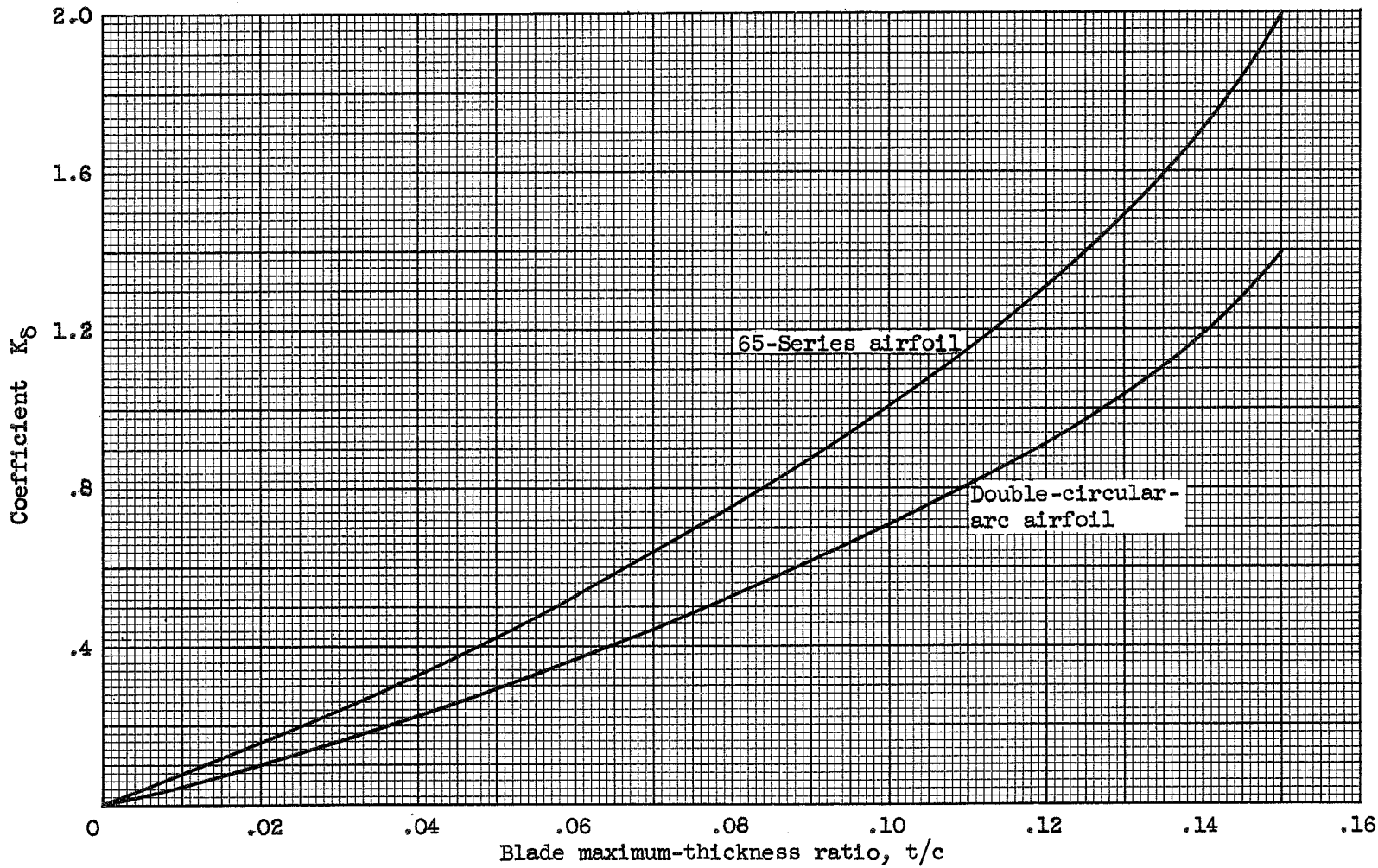
Figure 15. - Thickness correction for zero-camber deviation angle (ref. 4).
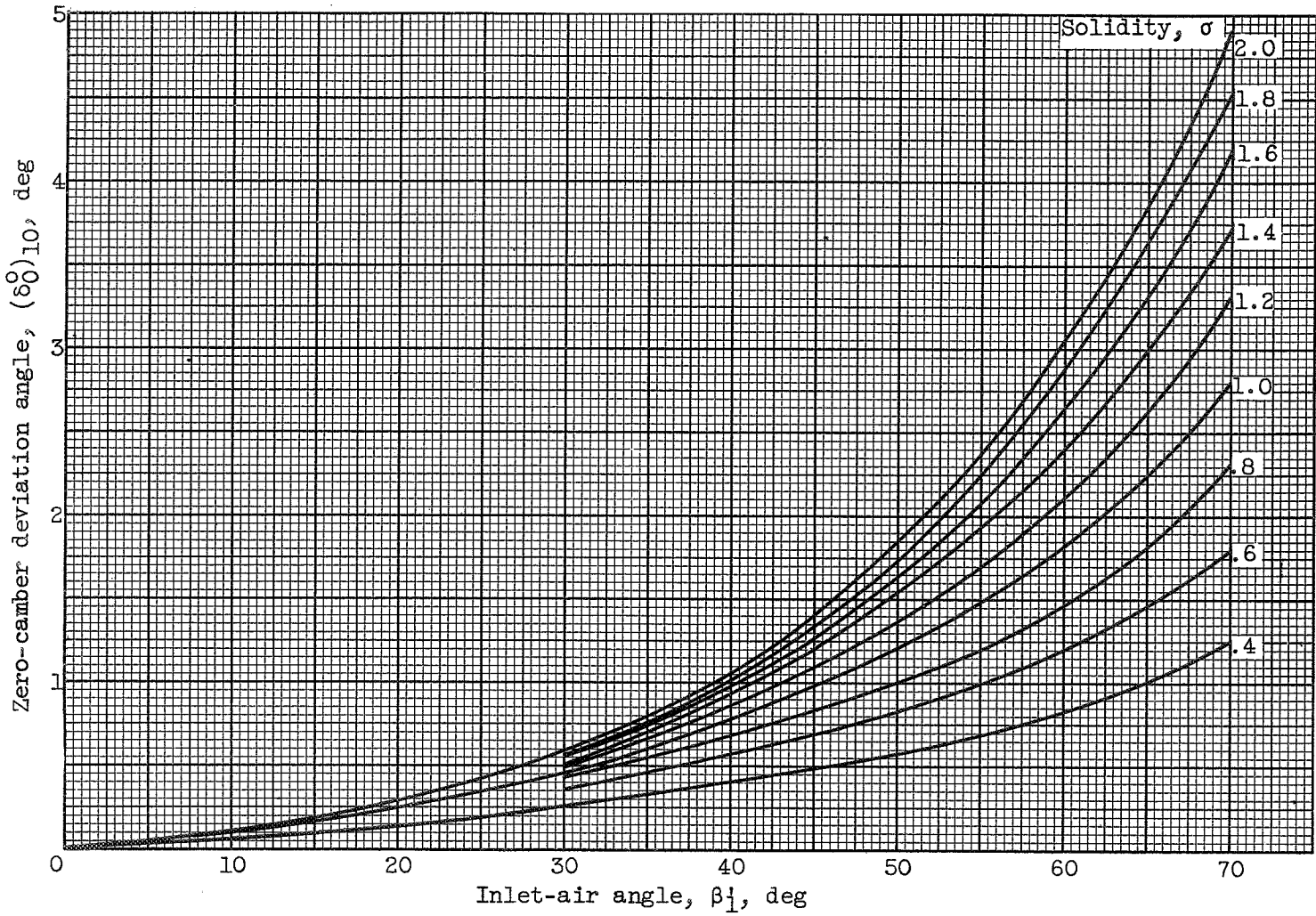
Figure 16. - Zero-camber deviation angle for NACA 65-series and true circular-arc blades of 10-percent maximum-thickness ratio (ref. 4).
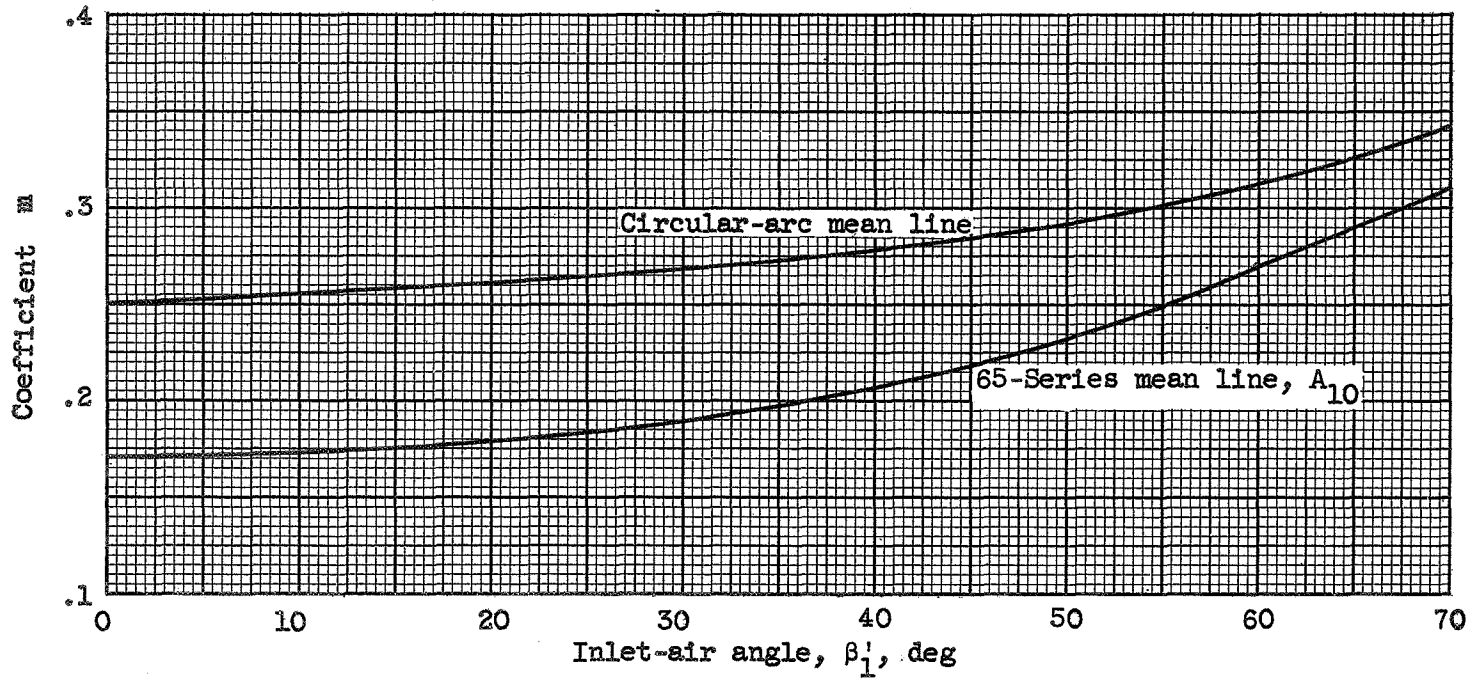
Figure 17. - Coefficient of m in deviation rule (ref. 4).
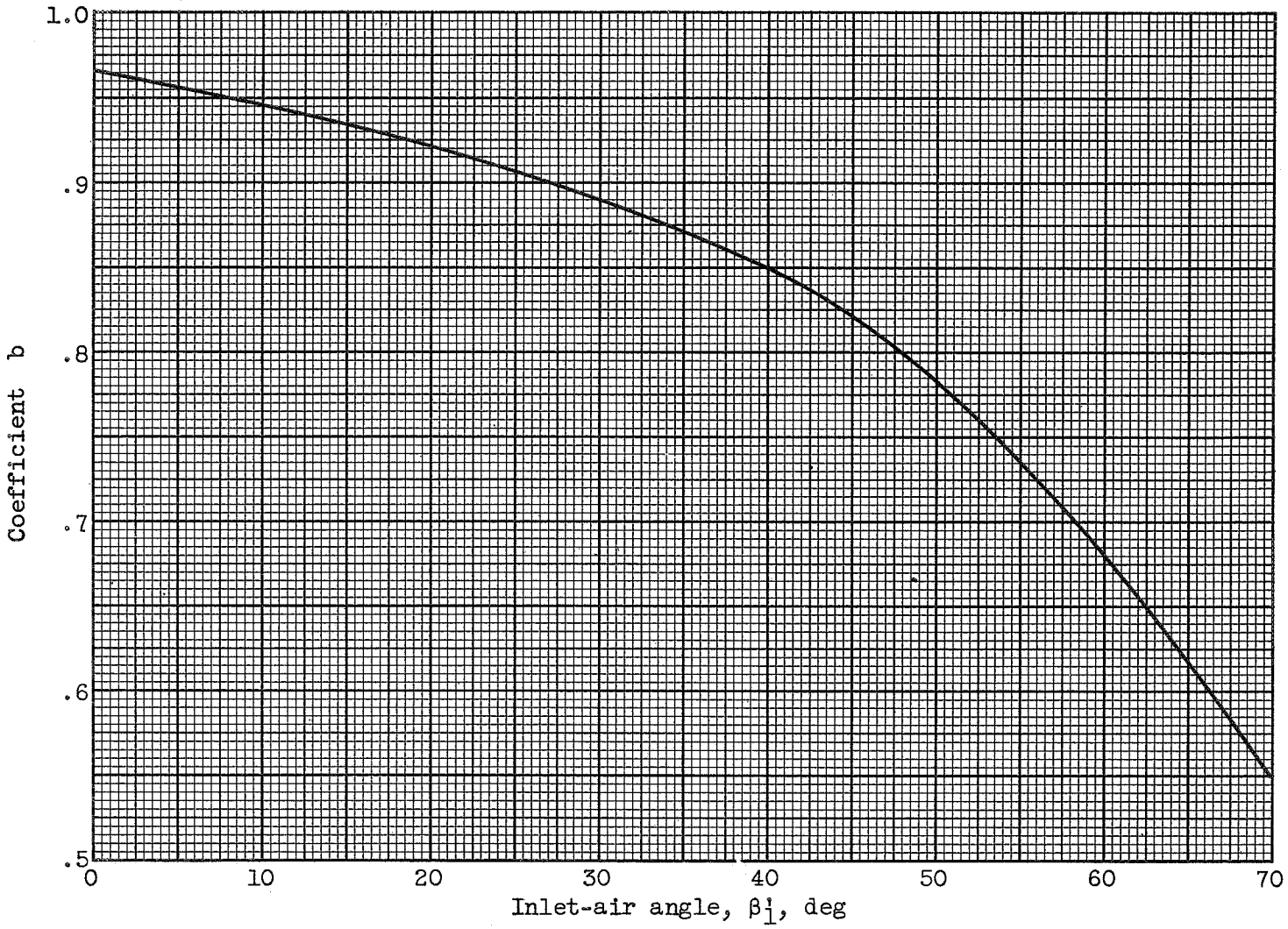
Figure 18. - Solidity exponent b in deviation rule (ref. 4).
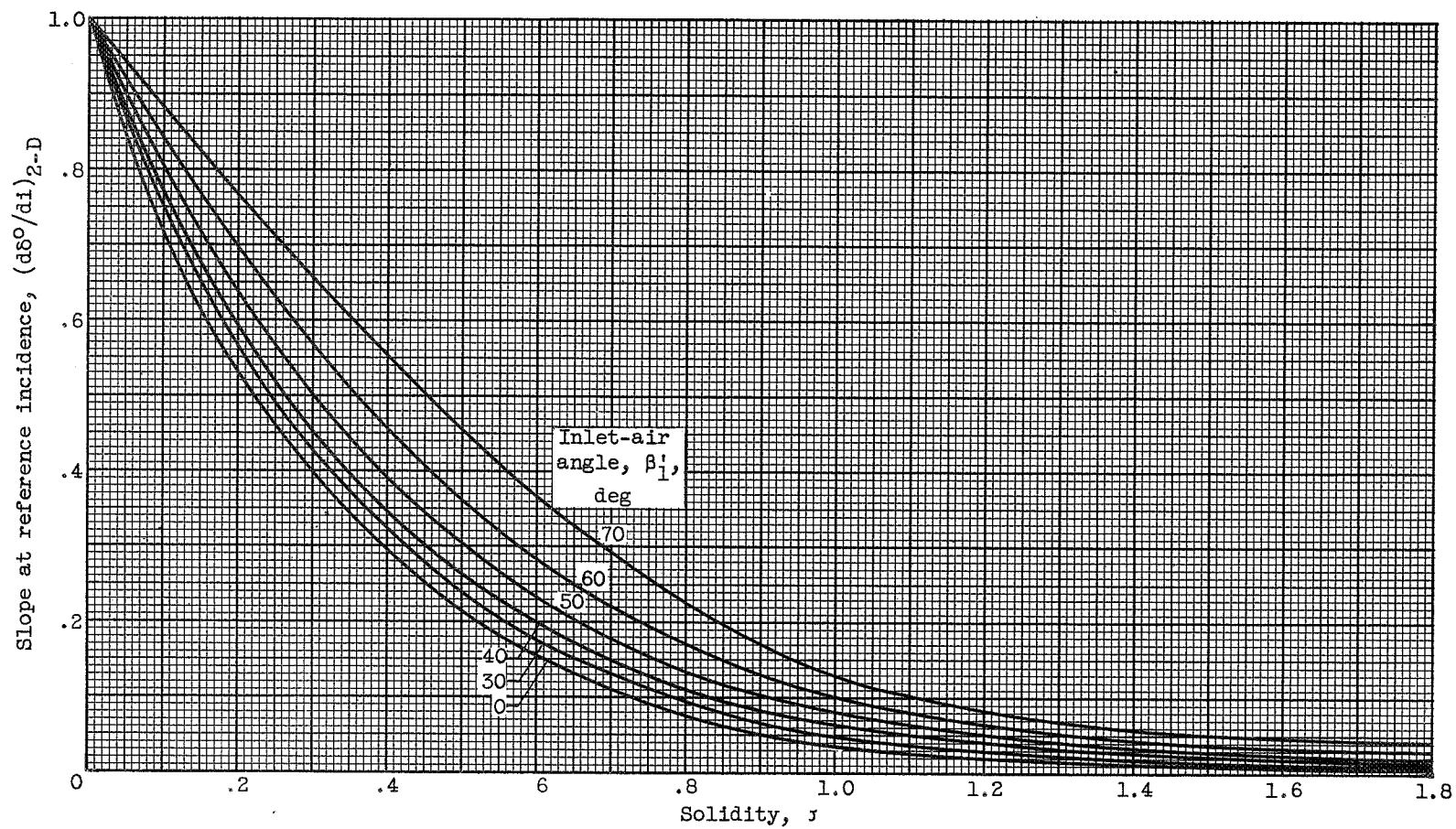
Figure 19. - Deviation-angle slope $(d\delta^o/di)_{2-D}$ at reference incidence angle (ref. 4).
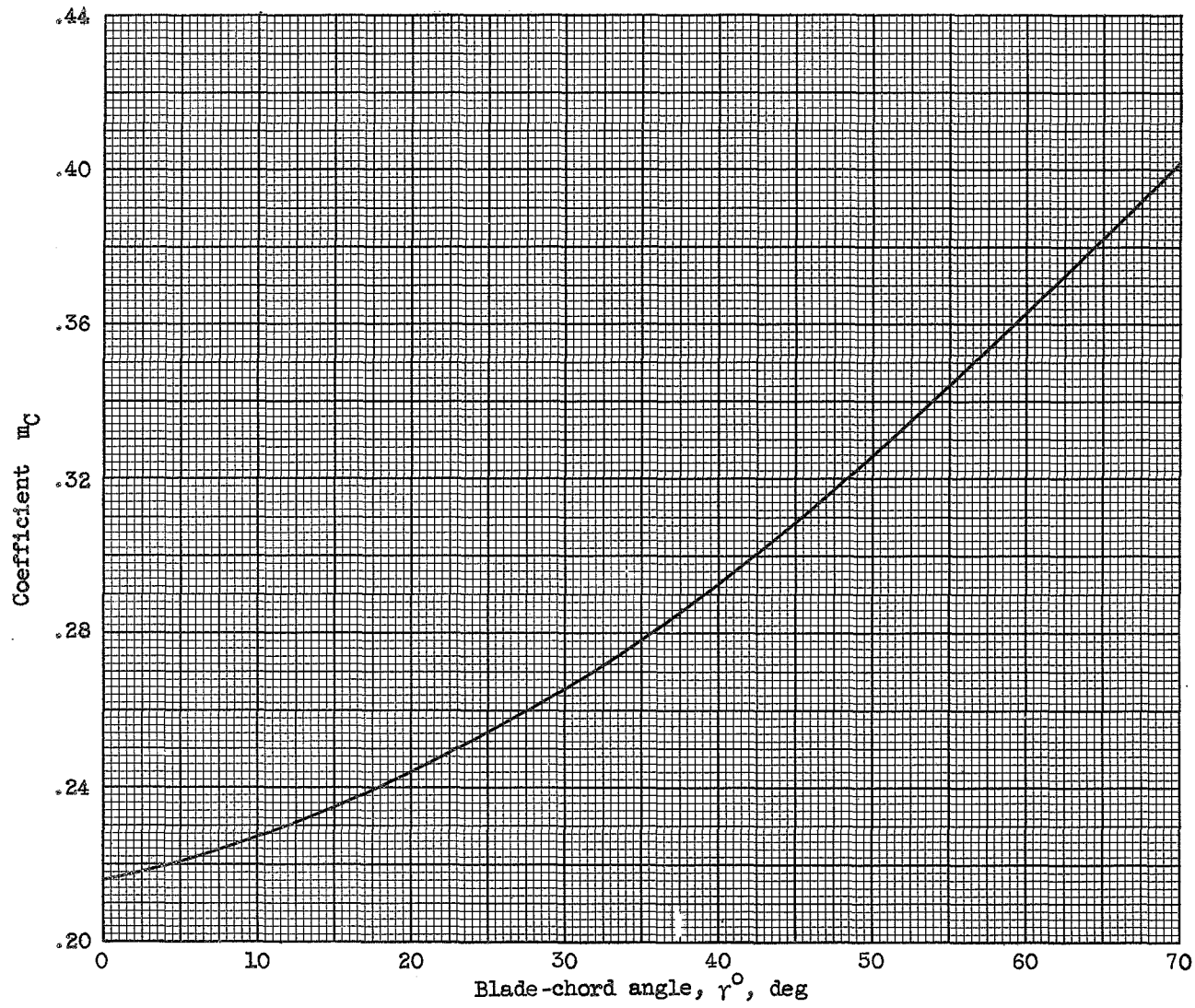
Figure 20. - Variation of m_C for circular-arc compressor cascades (ref. 31).
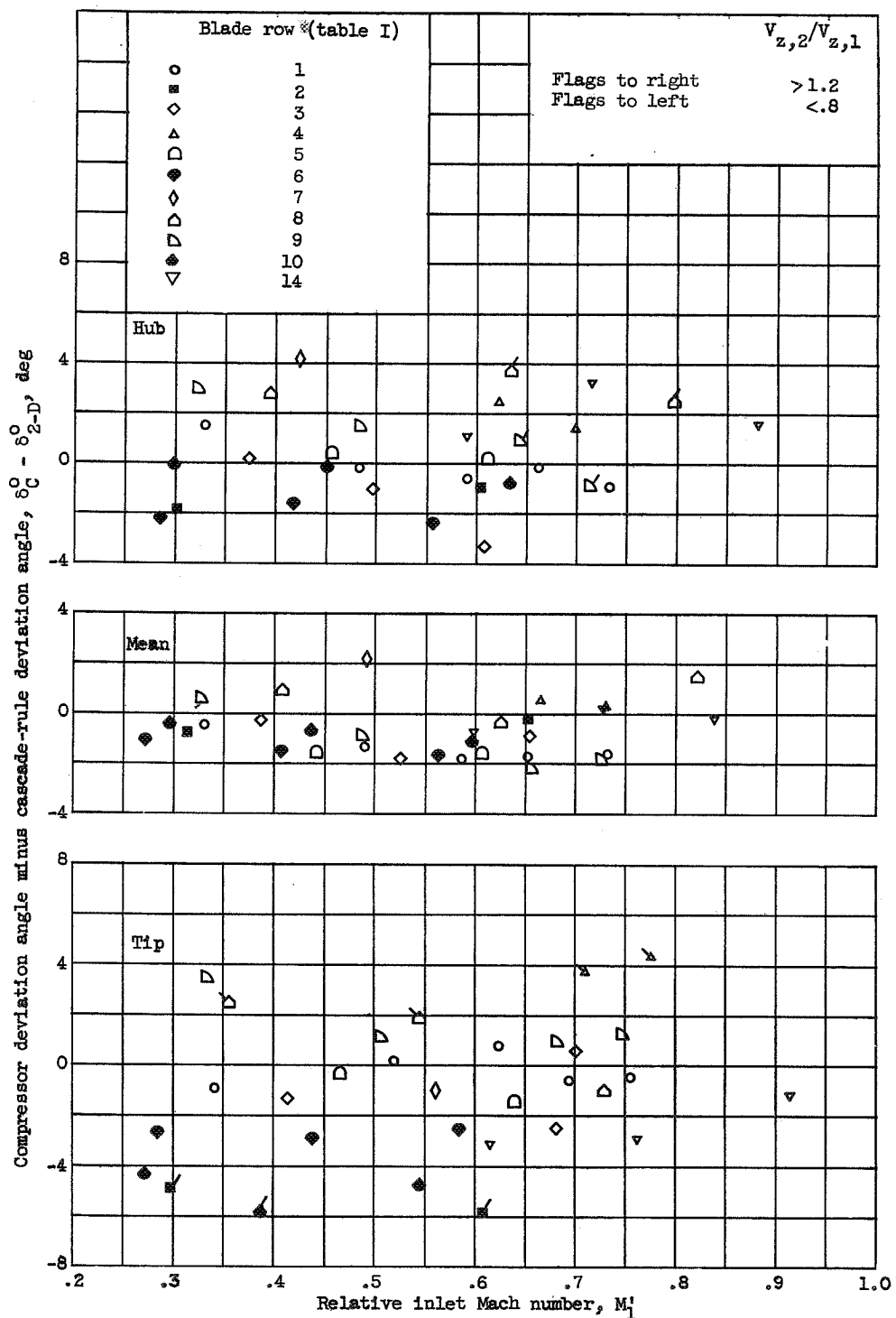
(a) 65(A$_{10}$)-Series blade section.

Figure 21. - Variation of compressor deviation angle minus two-dimensional-cascade deviation angle at compressor reference incidence angle with relative inlet Mach number.
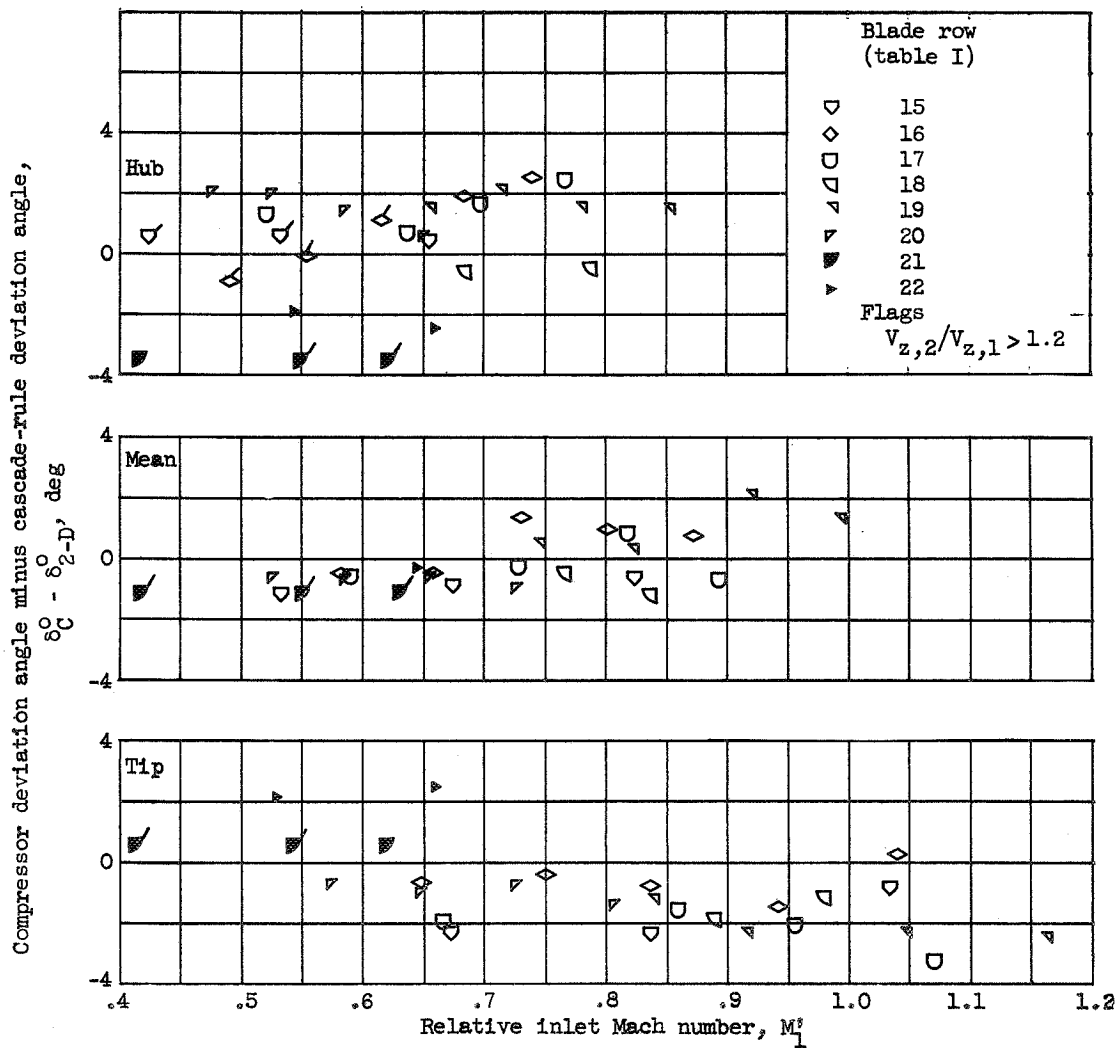
(b) Circular-arc blade section.

Figure 21. - Concluded. Variation of compressor deviation angle minus two-
dimensional-cascade deviation angle at compressor reference incidence
angle with relative inlet Mach number.
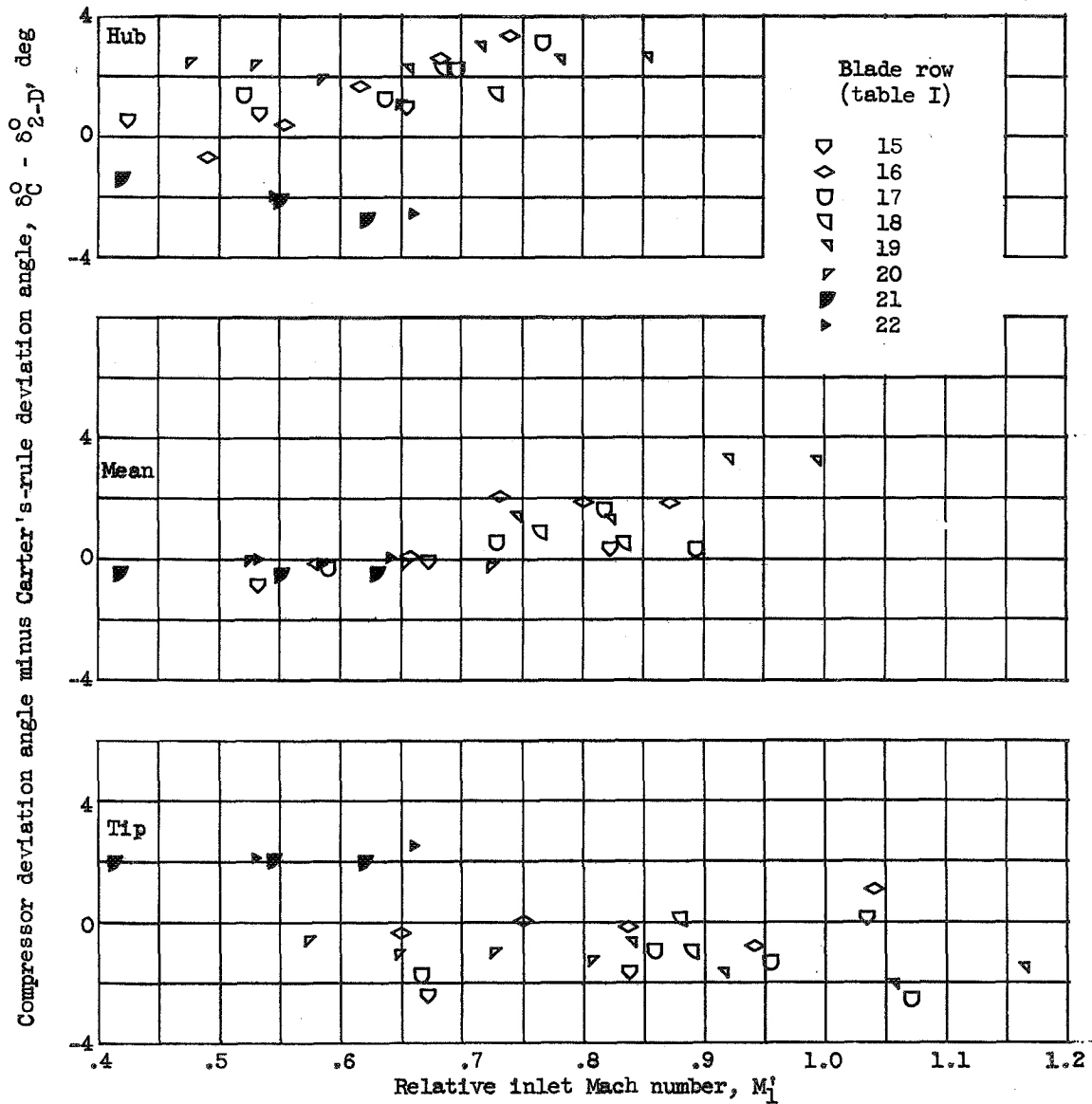
Figure 22. - Variation of compressor deviation angle minus deviation angle predicted by Carter's rule at reference incidence angle with relative Mach number for double-circular-arc blade section.
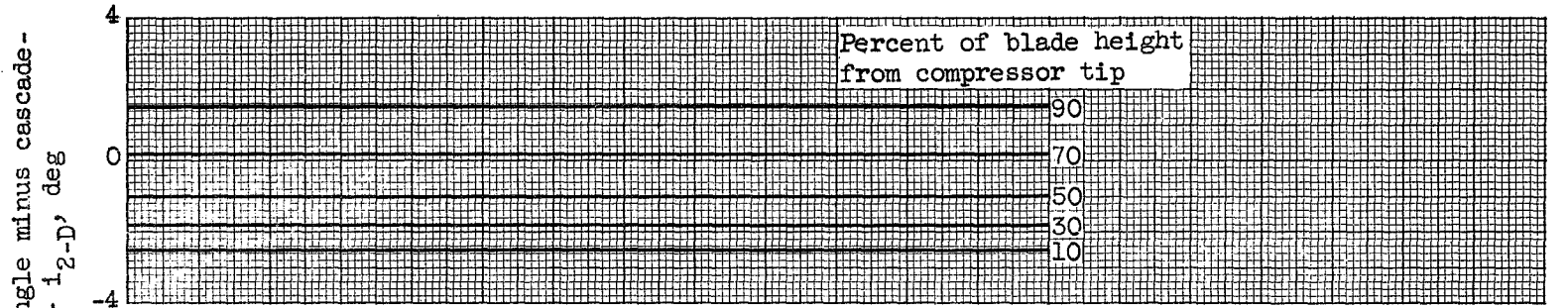
(a) NACA 65(A_{10})-series blades.
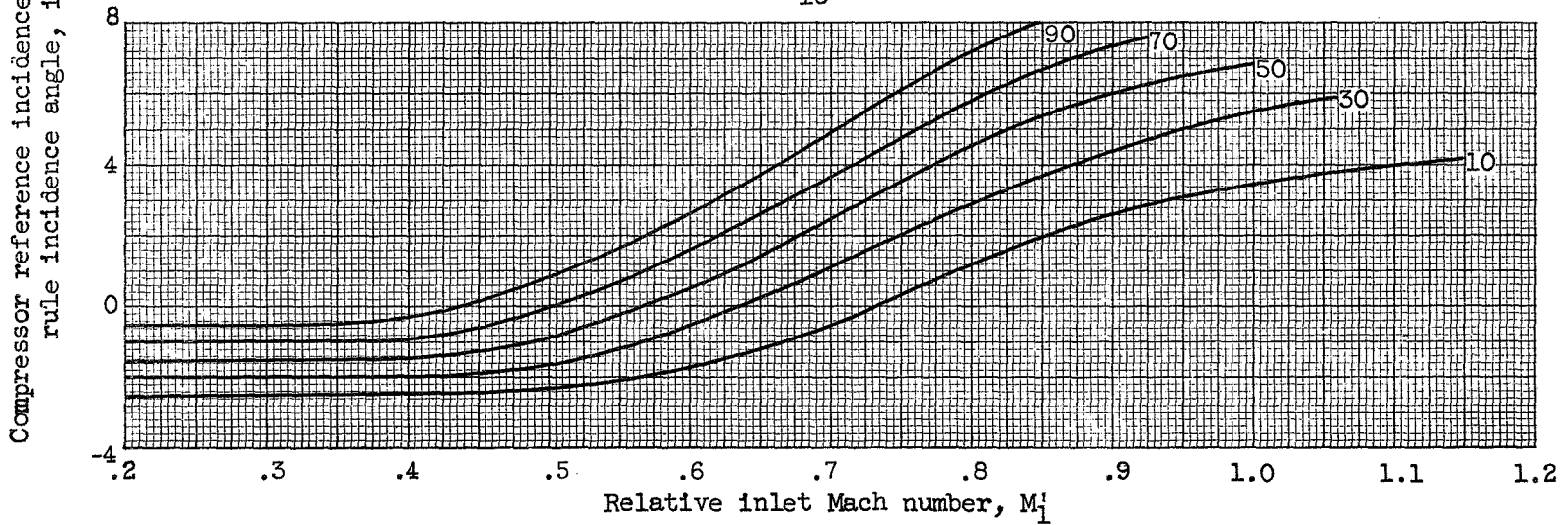
(b) Double-circular-arc blades.

Figure 23. - Deduced variation of average rotor reference incidence angle minus low-speed two-dimensional-cascade-rule reference incidence angle with inlet Mach number.

(a) NACA 65(A_{10})-series blades.

(b) Double-circular-arc blades.
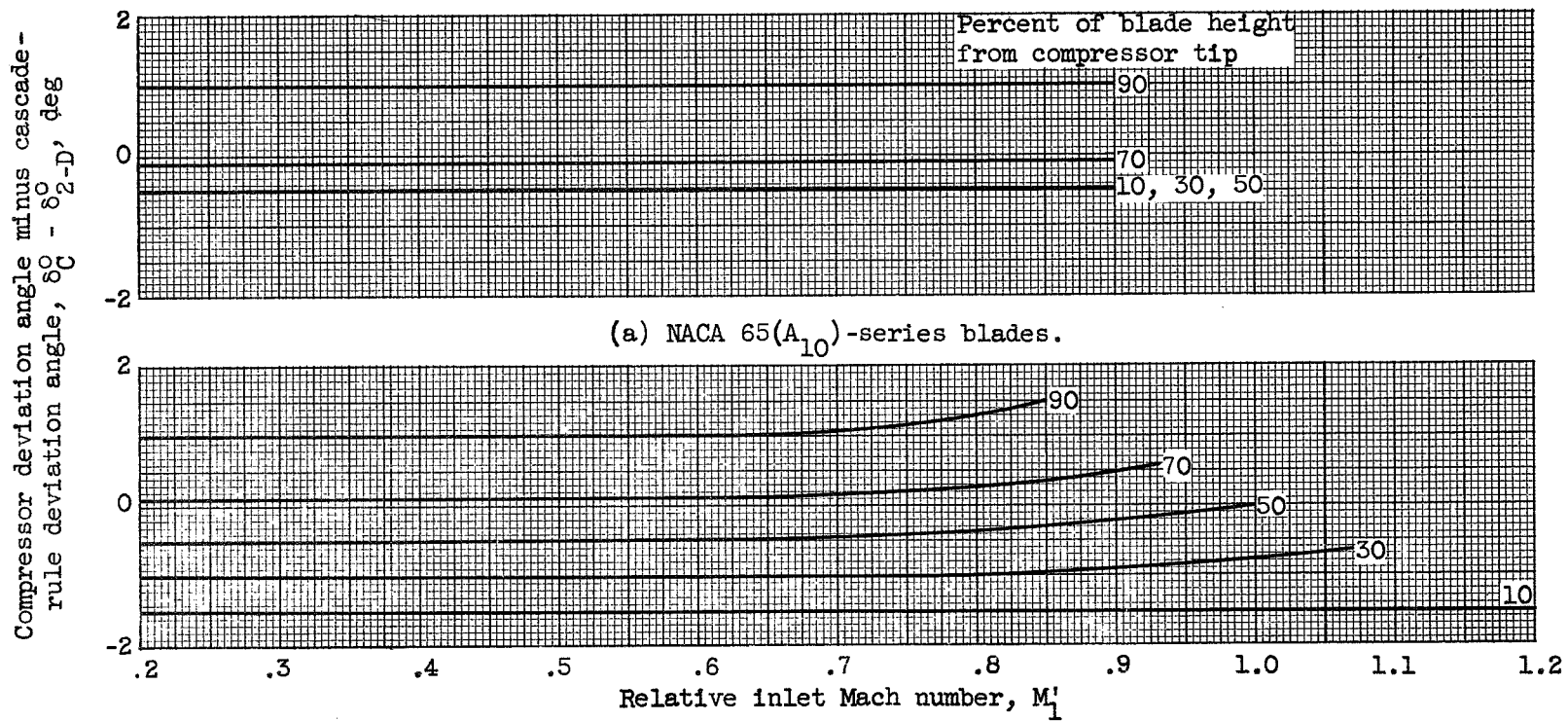
Figure 24. - Deduced variation of average rotor deviation angle minus low-speed two-dimensional-cascade-rule deviation angle at compressor reference incidence angle with relative inlet Mach number.

(a) Rotor

(b) Stator.
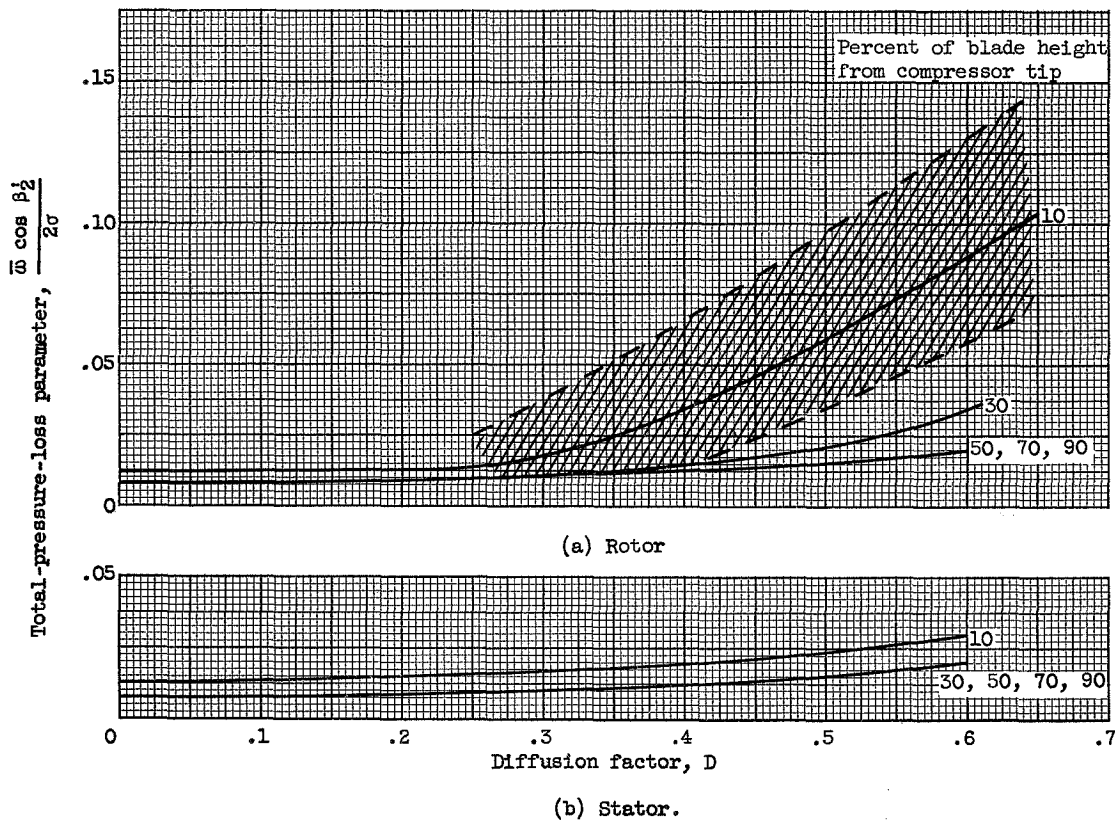
Figure 25. - Deduced variation of total-pressure-loss parameter with diffusion factor at reference incidence angle for NACA $65(A_{10})$-series and double-circular-arc blades.

Relative inlet
Mach number,
M_1'
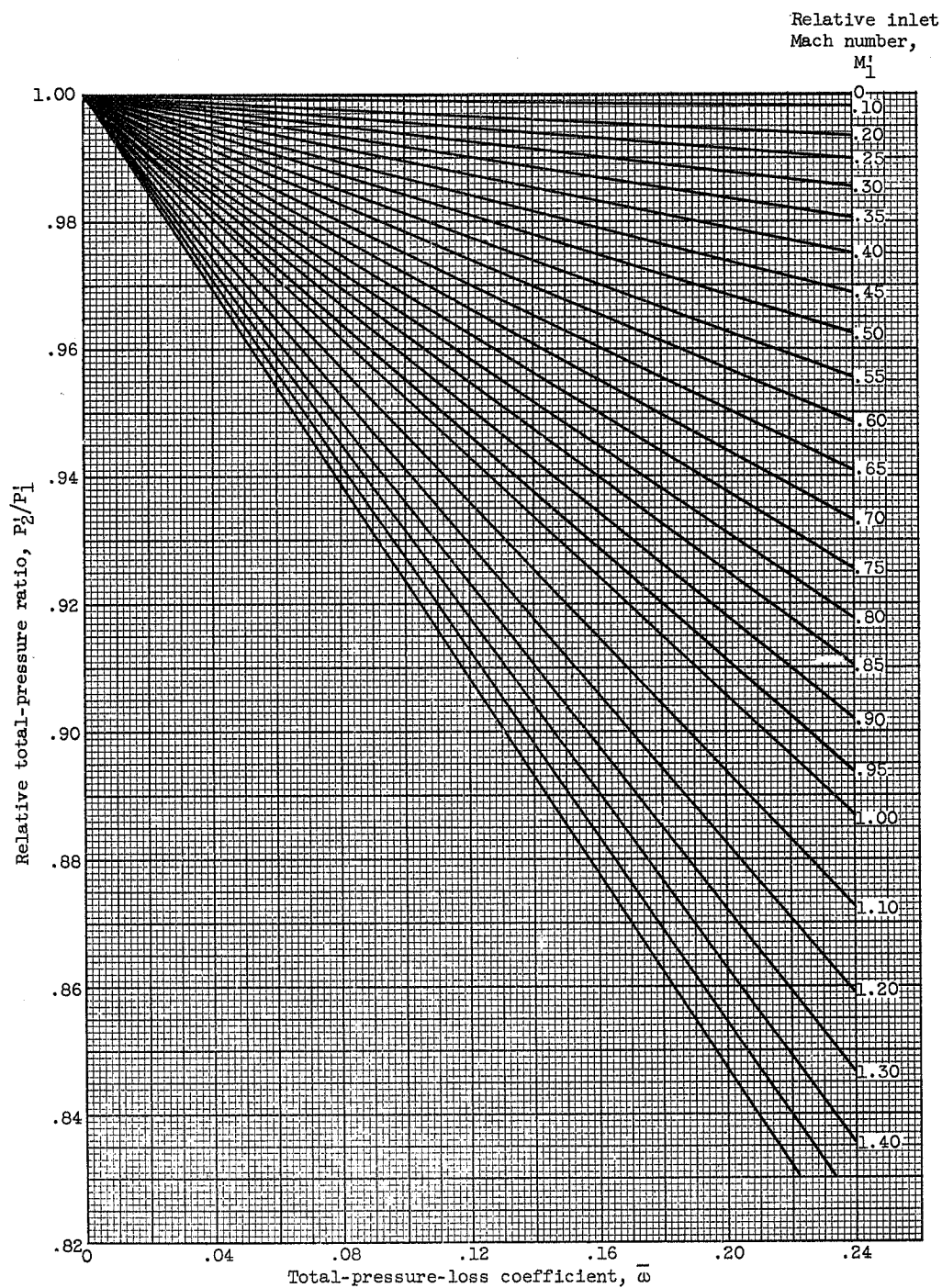
Figure 26. - Variation of rotor relative total-pressure ratio with total-pressure-loss coefficient and inlet Mach number.

$$\bar{\omega} = \frac{1 - \dfrac{P_2'}{P_1'}}{1 - \dfrac{1}{\left[1 + \dfrac{\gamma-1}{2}(M_1')^2\right]^{\frac{\gamma}{\gamma-1}}}}.$$

Rotor adiabatic efficiency
$\eta_{ad,R}$
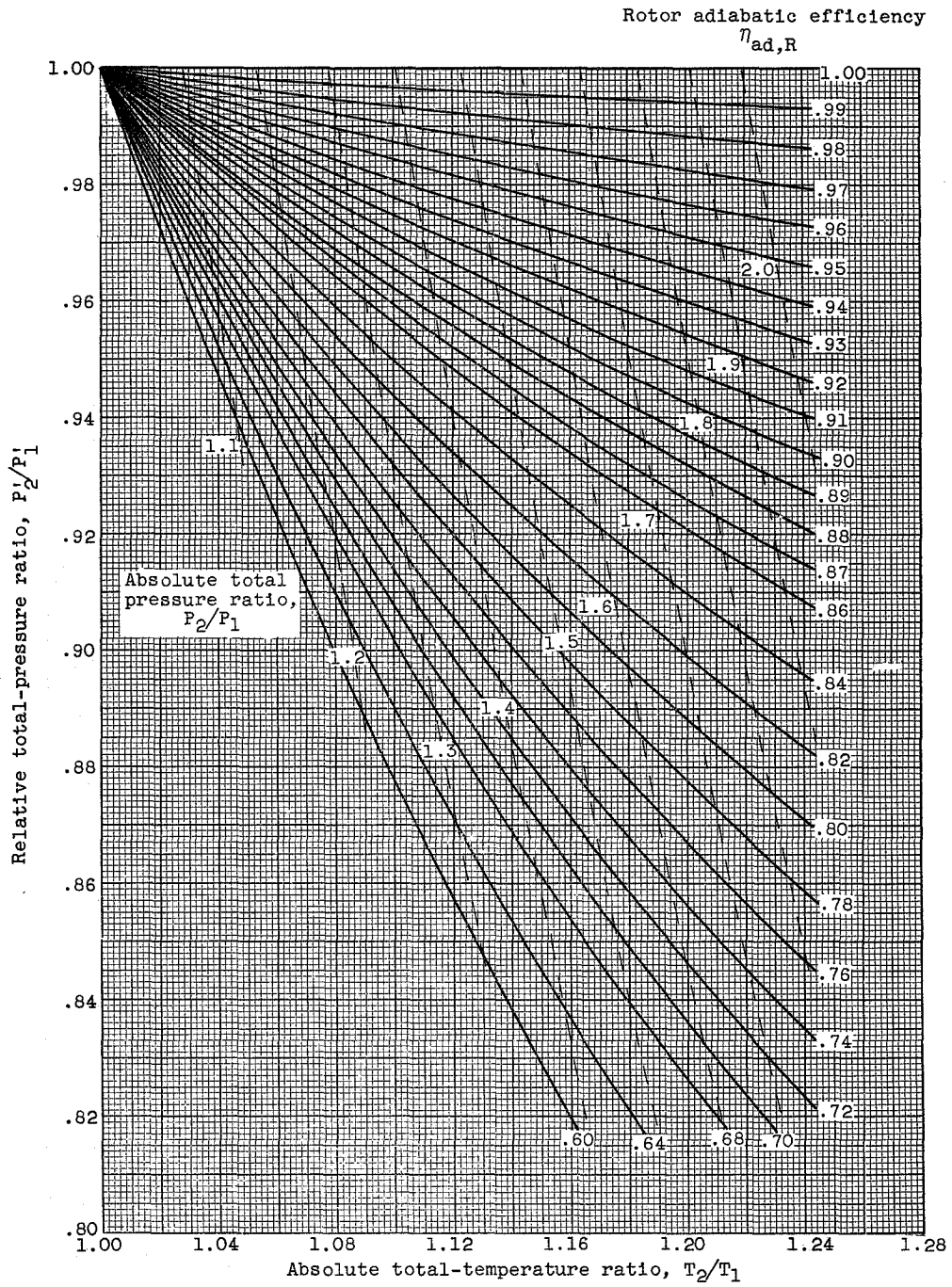
Figure 27. - Variation of relative total-pressure ratio with absolute
total-temperature ratio and efficiency for rotor.

$$\eta_{ad} = \frac{\left[\dfrac{P_2'}{P_1'}\left(\dfrac{T_2}{T_1}\right)^{\frac{\gamma}{\gamma-1}}\right]^{\frac{\gamma-1}{\gamma}} - 1.0}{\dfrac{T_2}{T_1} - 1.0}$$
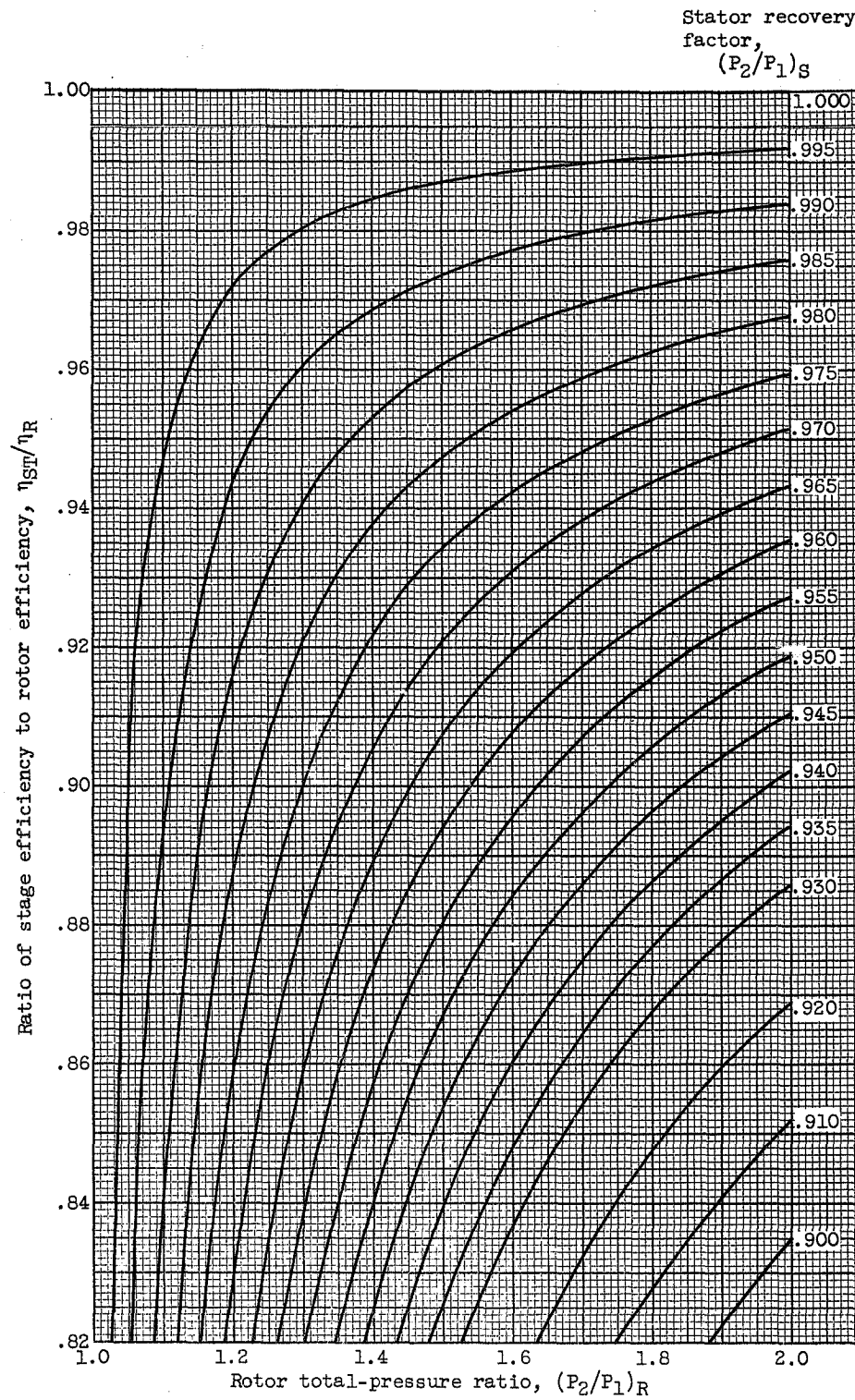
Figure 28. - Variation of ratio of stage to rotor efficiency with rotor absolute total-pressure ratio as function of stator recovery factor.

CONFIDENTIAL

AERODYNAMIC DESIGN OF AXIAL-FLOW COMPRESSORS

VII - BLADE-ELEMENT FLOW IN ANNULAR CASCADES

William H. Robbins
Aeronautical Research Scientist
Compressors and Turbines

Robert J. Jackson
Aeronautical Research Scientist
Compressors and Turbines

Seymour Lieblein
Aeronautical Research Scientist
Compressors and Turbines

Approved:

William A. Benser
Aeronautical Research Scientist
Compressors and Turbines

Robert O. Bullock
Aeronautical Research Scientist
Compressors and Turbines

Oscar W. Schey
Chief, Compressor and Turbine
Research Division

cwk - 8/9/55

CONFIDENTIAL

CONFIDENTIAL

Robbins, William H., Jackson, Robert J., and Lieblein, Seymour

AERODYNAMIC DESIGN OF AXIAL-FLOW COMPRESSORS
VII - BLADE-ELEMENT FLOW IN ANNULAR CASCADES

Abstract

Annular blade-element data obtained primarily from single-stage compressor installations are correlated over a range of inlet Mach numbers and cascade geometry. The correlation curves are presented in such a manner that they are related directly to the low-speed two-dimensional-cascade data of part VI of this series. Thus, the data serve as both an extension and a verification of the two-dimensional-cascade data. In addition, the correlation results are applied to compressor design.

CONFIDENTIAL